LARGE EDDY SIMULATIONS OF ISOTHERMAL AND NON-ISOTHERMAL TURBULENT FLOWS FOR HIGH TEMPERATURE GAS COOLED REACTORS

by

Sasan Salkhordeh

Submitted to the Graduate Faculty of

Swanson School of Engineering in partial fulfillment

of the requirements for the degree of

Doctorate of Philosophy

University of Pittsburgh

2015

www.manaraa.com

ProQuest Number: 10075429

All rights reserved

INFORMATION TO ALL USERS
The quality of this reproduction is dependent upon the quality of the copy submitted.

In the unlikely event that the author did not send a complete manuscript
and there are missing pages, these will be noted. Also, if material had to be removed,
a note will indicate the deletion.

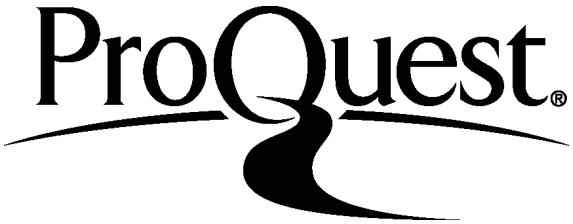

ProQuest 10075429

Published by ProQuest LLC (2016). Copyright of the Dissertation is held by the Author.

All rights reserved.
This work is protected against unauthorized copying under Title 17, United States Code
Microform Edition © ProQuest LLC.

ProQuest LLC.
789 East Eisenhower Parkway
P.O. Box 1346
Ann Arbor, MI 48106 - 1346

www.manaraa.com

UNIVERSITY OF PITTSBURGH

SWANSON SCHOOL OF ENGINEERING

This dissertation was presented

by

Sasan Salkhordeh

It was defended on

November 17, 2015

and approved by

Laura Schaefer, PhD., Professor, Department of Mechanical Engineering, Rice University

John Brigham, PhD., Associate Professor Department of Civil and Environmental Engineering, University of Pittsburgh

Anirban Jana, PhD., Senior Scientific Specialist, Pittsburgh Supercomputing Center, Carnegie Mellon University

Dissertation Director: Mark Kimber, PhD., Assistant Professor, Department of Mechanical Engineering and Material Science, University of Pittsburgh

www.manaraa.com

Copyright © by Sasan Salkhordeh

2015

www.manaraa.com

LARGE EDDY SIMULATIONS OF ISOTHERMAL AND NON-ISOTHERMAL TURBULENT FLOWS FOR HIGH TEMPERATURE GAS COOLED REACTORS

Sasan Salkhordeh, PhD

University of Pittsburgh, 2015

In order to develop an experimentally validated computational model for the lower plenum of High Temperature Gas-Cooled Reactors (HTGR), three separate Large Eddy Simulation (LES) studies are conducted. First, detailed study is made of LES for an isothermal turbulent jet, which is compared to well-accepted experimental data. Inconsistencies in the literature surrounding the Reynolds number dependence for the turbulent statistics are comprehensively addressed. Second, a non-isothermal LES study of flow over a cylinder is conducted, and includes comparison between experimental data and LES for different subcritical Reynolds numbers. The final study is that of LES for a non-isothermal round jet, where the effect of a precursor simulation is found to play a vital role for capturing the underlying physics within the turbulent Navier Stokes and energy equations. Good agreement is obtained between our LES predictions and experimental measurements in both near-field and far-field data. This research lays the groundwork needed to develop high-fidelity, experimentally validated computational models of the complex mixing flow in the HTGR lower plenum.

www.manaraa.com

TABLE OF CONTENTS

www.manaraa.com

www.manaraa.com

LIST OF TABLES

www.manaraa.com

LIST OF FIGURES

www.manaraa.com

www.manaraa.com

www.manaraa.com

www.manaraa.com

ACKNOWLEDGMENTS

I would like to express my sincere appreciation to my advisor, Dr. Mark Kimber for his support and guidance through the course of my research. My appreciation also goes to Dr. Anirban Jana for his collaboration on many technical aspects of my research. I owe special thanks to Dr. Sagnik Mazumdar whose insight and help contributed greatly to the quality of my research. I am also grateful to my colleagues and friends at the University of Pittsburgh, Tyler Landfried, Corey Clifford, Paul Kristo, Greg Stehle and Ricardo Rivera-Lopez. I am also thankful of Dr. Peyman Givi, Dr. Mehdi Nik and Dr. Patrick Pisciuneri for their friendship and assistance during my years in graduate school. My deepest gratitude goes to my parents and brothers for their love and support.

This research is being performed using funding received from the DOE Office of Nuclear Energy's Nuclear Energy University Programs.

www.manaraa.com

1.0 INTRODUCTION AND MOTIVATION

Computational Fluid Dynamics (CFD) has become a standard modeling approach for many industries. It provides the engineer with the opportunity to conduct detailed investigations where the only expense is a computational one. Flow features can also be thoroughly investigated in a non-invasive way, as opposed to experimental techniques which almost always require some amount of intrusion into the flow. However, these significant advantages of CFD must be viewed with some degree of skepticism, especially for complex or turbulent flows, where a given modeling approach, although numerically stable and able to produce seemingly reasonable results, may not be physically valid depending on the underlying assumptions on which it is based. Recognizing these limitations, there has been a concerted effort over the past number of decades to establish formal guidelines one can use to quantify the uncertainty of CFD generated results [1, 2]. Verification and Validation (V&V) and Uncertainty Quantification (UQ) are now commonly used terms in computational circles. The importance of this topic is evident given the fact that ASME has created a new Journal of Verification, Validation and Uncertainty Qualification with the first publications planned for 2016, as well as established an annual symposium dedicated to V&V. Attendees from both academia and industry represent a wide breadth of important applications such as nuclear, medical, space science, instrumentation & controls and defense to name a few.

www.manaraa.com

In the nuclear field, simulations are routinely run to predict static and dynamic plant performance under normal conditions and accident scenarios. The level of trust one can adopt for these simulations is intimately tied to the degree the code has been vetted with V&V. Detailed procedures exist for current reactor technologies, where the simulations rarely require full CFD modeling. For next generation reactors however, CFD will become a much more integral component of the plant simulations. The focus of this research is to address the V&V needs for CFD related physics in next generation reactors by providing validated 3D numerical models for the flow physics important to the High Temperature Gas Cooled Reactor (HTGR). In order to outline the specific contribution made by this research, V&V will be discussed in more detail, followed by an in depth look at the CFD needs for HTGRs.

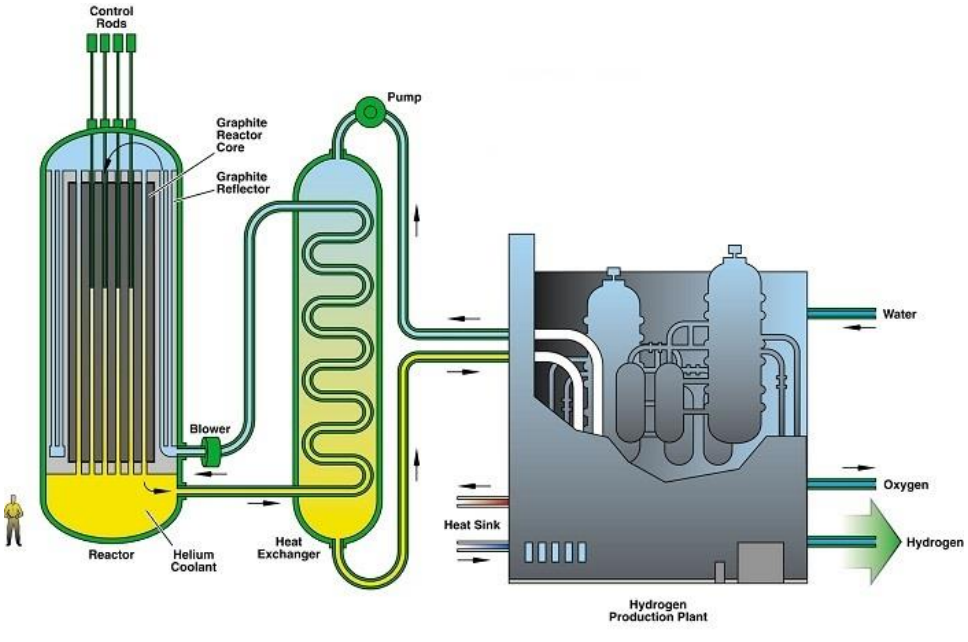

Figure 1. VHTR with electricity and hydrogen production alternatives [3]

www.manaraa.com

1.1 HIGH TEMPERATURE GAS COOLED REACTOR (HTGR)

The Very High Temperature Reactor (VHTR) is a Generation IV reactor which enables high-efficiency production of electricity, hydrogen, or process heat (Figure 1). The VHTR is the most likely candidate for the Next Generation Nuclear Plant [4].For successful implementation, it is essential to address several performance and safety issues related to thermal hydraulics of the VHTR [5].

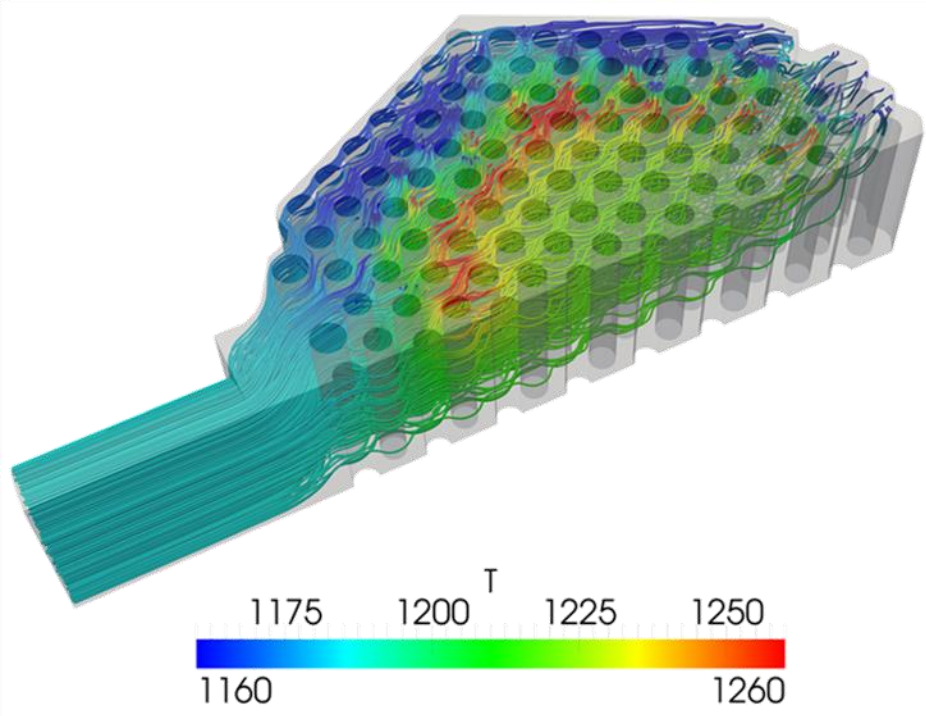

Figure 2. CFD predictions of flow paths and temperatures in a computer model of the lower plenum of a VHTR [6]

www.manaraa.com

1.2 COMPUTATIONAL MODELING OF FLOW CONDITION IN LOWER PLENUM OF VHTRS

Several investigations have been conducted over the last decade primarily focusing on the flow characteristics in scaled models of the VHTR lower plenum under isothermal conditions [7, 8]. However, in reality, the helium coolant jets enter the lower plenum at vastly different temperatures from the non-uniformly heated core where turbulent mixing occurs. It is a complex mixing flow, where the array of jets with inlet velocities ranging from 50 to 100 m/s and temperature spreads as high as 300°C, turn 90° and merge into a single outlet flow while negotiating a bank of cylindrical supports. Because of the high operating temperatures of the VHTR, it is important to ensure that large temperature gradients are not present in the lower plenum as it would potentially impact the structural materials. Presently, efforts are being made to understand the non-isothermal flow hydrodynamics in the lower plenum of the VHTR. Detailed experimental and computational investigations of the non-isothermal flow are currently being planned for locations A, B and C of the lower plenum (Figure 3) in the Kimber lab at the University of Pittsburgh. The primary objective of this extensive experimental and computational research is to build accurate computational models of VHTR thermal-hydraulic phenomena and to generate benchmark data for assessment and improvement of VHTR design. However, to model the flow with reasonable accuracy, it is essential to have a primary understanding of the flow characteristics for the benchmark prototypes.

www.manaraa.com

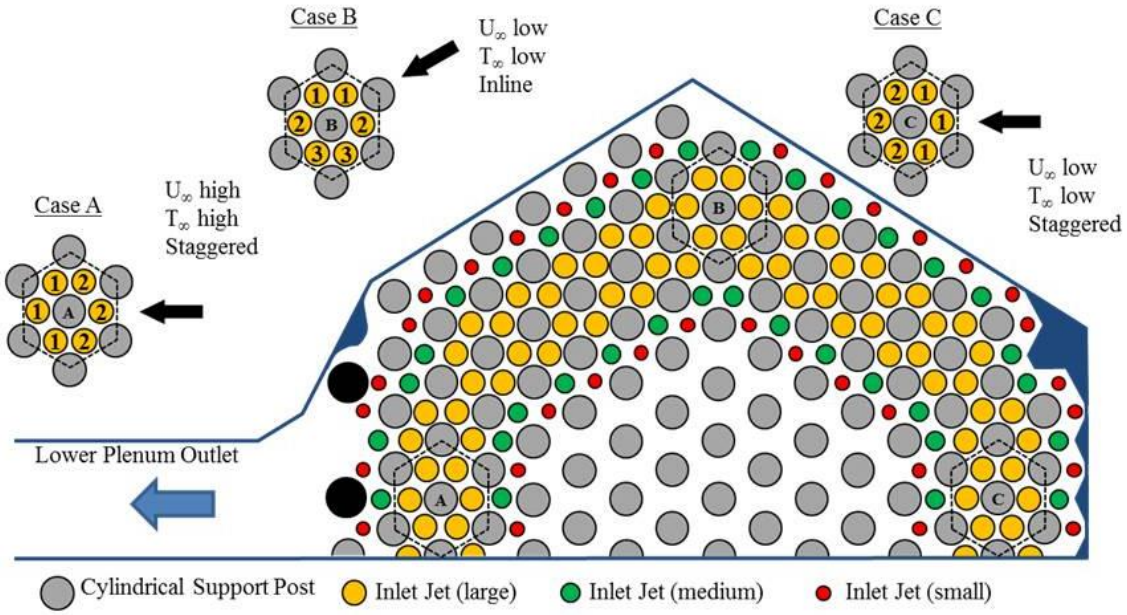

Figure 3. Unit Cell for studying the lower plenum of the VHTR

Although approaching the problem with a RANS method provides useful insight under different scenarios, for such high Reynolds number flows where detailed spatial and temporal physics are of interest, the Large Eddy Simulation (LES) represents the most logical approach to address the key characteristics of thermal hydraulic behavior in lower plenum of the VHTR.

1.2.1 Thermal striping in HTGRs

The turbulent mixing of multiple jet streams of different temperatures raises major concerns regarding structural failure due to thermal fatigue, which is enabled when temperature fluctuations in fluid flow are transmitted to the support structure. This phenomenon by which

www.manaraa.com

temperature fluctuations in the fluid are transported into and attenuated by the support structure is known as thermal striping.

In order to more fundamentally understand the complicated flow and its influence on thermal striping in the lower plenum, it must be broken down into manageable subcomponents, where detailed experimental and computational studies can more easily be accomplished. The goal of this thesis is to computationally model these benchmarks in order to better quantify the physics behind thermal striping in the lower plenum. Three specific scenarios are investigated: (i) isothermal turbulent jet, (ii) turbulent flow past a heated cylinder, and (iii) non-isothermal turbulent jet. For each scenario, the models are compared to well-accepted experimental results. With validated LES models, greater understanding of the flow physics is possible, and groundwork is laid for establishing V&V approaches for LES. The contributions made in this thesis therefore have impact on future model development for the VHTR lower plenum, but also deliver trusted results for several canonical flows, which enables future investigators to develop a formal uncertainty quantification framework. Therefore, three key contributions are made in this thesis:

- **Greater understanding of turbulence statistics for fundamental turbulent flows, both isothermal and non-isothermal.**
- **Detailed computational results to inform V&V efforts in the VHTR lower plenum.**
- **Foundation with trusted data for quantifying uncertainty in LES models.**

The remainder of this thesis provide details of the LES models for the three flow scenarios considered, namely an isothermal turbulent jet, flow past a heated cylinder, and a non-isothermal

www.manaraa.com

turbulent jet. Chapter 2 provides details of the completed work for an isothermal turbulent jet, which is compared to well-accepted experimental data. As will be shown, inconsistencies in the literature surrounding the Reynolds number dependence for the turbulent statistics has been comprehensively addressed. Chapter 3 then delivers a non-isothermal large eddy simulation study of flow over a cylinder and includes comparison between experimental data and LES for different subcritical Reynolds numbers. Finally, Chapter 4 completes the framework with providing LES studies of a non-isothermal round jet. In this chapter the effect of precursor simulation is found to play vital role for capturing physics of the problem. All LES results are in excellent agreement with well-known experimental studies available in the literature.

www.manaraa.com

2.0 LARGE EDDY SIMULATION OF AN ISOTHERMAL TURBULENT ROUND JET

The lower plenum of the High Temperature Gas-Cooled Reactor (HTGR) is an extremely complex non-isothermal flow. In the direction of developing an experimentally validated computational model for the lower plenum flow, the flow is broken down into fundamental processes for detailed validation. The most fundamental flow condition of interest is a round turbulent jet. In this chapter, a Large Eddy Simulation (LES) of an isothermal high Reynolds number confined jet is presented. The enclosure within which the jet is confined is selected large enough so that the results can be compared with well-known experimental studies available in the literature. Detailed comparisons are made with experimental data for the velocities and higher order moments and excellent agreement is found in all cases. With a fully validated numerical model, additional insight is also provided in terms of the turbulent kinetic energy budget, as noted in Section 2.3.3, which helps resolve inconsistencies in the current literature.

2.1 INTRODUCTION

The turbulent mixing of non-isothermal jets is the source of the temperature fluctuations leading to thermal fatigue in the lower plenum of the HTGR. The temperature fluctuations directly produced by turbulence are non-coherent. In addition, coherent fluctuations may be superimposed

www.manaraa.com

under certain conditions [9]. LES models can capture with sufficient accuracy both the turbulent and coherent fluctuations, and is therefore of great interest in such an application. However, fundamental work is still needed which addresses the modeling requirements to capture the important physics. LES explicitly solves the large, energy containing scales of turbulence that have a strong dependence on the specifics of each flow, while modeling the smaller, dissipative scales that have a more universal character [10, 11]. In contrast, Unsteady Reynolds Averaged Navier-Stokes (URANS) models cannot capture the details of the non-coherent fluctuations (e.g., its spectral content), while Direct Numerical Simulation (DNS) of the lower plenum would be prohibitively expensive.

The most widely used experimental studies for CFD validation of isothermal round jets are the works of Panchapakesan & Lumley (P&L) [12], Wygnanski & Fiedler (W&F) [13] and Hussein et al. (HCG) [14]. P&L reported measurements for a jet with $Re = 1.1\times10^4$. In contrast, the Reynolds's number of incoming jets in the VHTR lower plenum are expected to exceed 8×10^4 [9]. It has been observed that flow characteristics can be vastly different between a $Re = 1.1\times10^4$ [12] jet and a $Re = 9.55\times10^4$ [14] jet as used by Hussein et al. [15, 16]. The jet Re for the experiments of W&F ($Re = 10\times10^4$) and HCG ($Re = 9.55\times10^4$) were similar. However, W&F used SHW (Stationary Hot Wires) for their measurements which give erroneous results for high turbulent intensity flow especially at locations far from the centerline of the jet. Hence the experimental LDA (Laser Doppler Anemometer) and FHW (Flying Hot Wire) measurements of HCG are used for the current validation study.

www.manaraa.com

A comprehensive LES study corresponding to HCG is noticeably absent from the literature. Studies like Kim & Choi [15], which investigated the effects of the jet inflow conditions on the downstream evolution of a circular jet for Reynolds numbers of 3600, 10^4, and 10^5, only used axial domain length of 18 *D* (*D* being the diameter of the jet) for Re = 10^5 jet (i.e., only the near-field). HCG did the bulk of their flow measurements in the self-similar far-field region, at a downstream axial location of 70 *D*, and therefore these authors could not make direct comparisons. Bogey & Bailly (B&B) [16] reported that the distance required to achieve self-similarity of flow in the LES is around 60 *D* from their simulations for a Re = 1.1×10^4 jet (similar to P&L's experimental measurement). Moreover, even though B&B performed LES simulations for an axial domain length of 75 *D*, they found that flow characteristics (Re = 1.1×10^4) were vastly different from HCG. In addition, their Reynolds number (Re = 1.1×10^4) is an order of magnitude less than that of HCG. The potential core length simulated was also much longer than what was observed in the experiments of P&L. In other words, although they matched the far-field (i.e., self-similar region), their near-field computational results were significantly different than the experimental data they meant to mimic. For many applications (HTGRs included), the domain of interest can be entirely comprised of the near-field region due to geometric constraints. Comprehensive and systematic LES modeling is needed to help resolve these discrepancies for isothermal jet flow. The work presented here uses an appropriate domain size for effective validation with experimental measurements and addresses the issue of potential core length for a high Reynolds's number turbulent jet similar to HCG. It also addresses the inconsistencies in the literature regarding the turbulent statistics.

www.manaraa.com

2.2 COMPUTATIONAL MODEL

The isothermal round jet computed by LES is compared to that of the jet studied experimentally by HCG with the jet Reynolds number $Re = \frac{U_{inlet}D}{\nu} = 95{,}000$, where U_{inlet} is the jet exit velocity, D is the jet diameter, and ν is the kinematic viscosity of air. In the experiments, they used a jet with D = 1 in, and the experimental jet facility was surrounded by a large enclosure. As shown in Figure 4(a), the nozzle of the jet was placed within the enclosure such that the distance of the back wall to the nozzle was 34 ft (408 D) and the distance from the nozzle to the downstream exit of the facility was 48 ft (576 D). The width of the domain was 16 ft (192 D). The jet was centered in the cross-section of the enclosure.

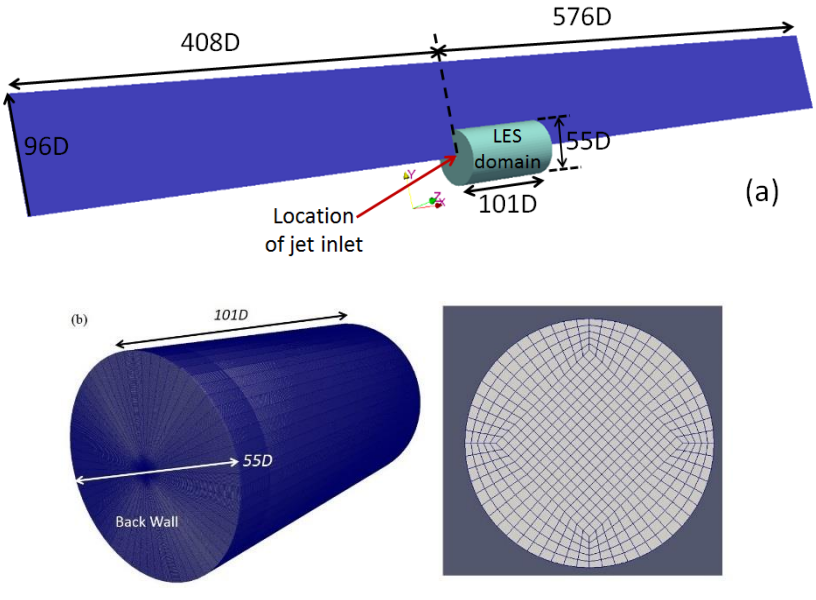

Figure 4. Comparison of the size of the LES simulation domain (R = 55 D/2) and HCG experimental domain (R = 96 D). The wedge geometry shown for the experimental domain is the axisymmetric domain (b) Views of the mesh near the inlet and at the side walls for the LES model.

www.manaraa.com

Simulating such a large domain is computationally prohibitive with LES. Hence a subset computational domain was simulated in the current study. The LES domain used for this study is shown in relation to the experimental HCG domain in Figure 4(a) and (b). The computational domain has dimensions of 101 *D* in the axial direction (100 *D* from jet inlet to the downstream outlet and 1 *D* from back wall to jet inlet) and 55 *D* in the radial direction. It should be noted that the downstream location of $x = 70\ D$ (location where detailed experimental results are reported in HCG) is within the LES computational domain. The radial dimension of the LES domain was selected based on an axisymmetric RANS simulation of the full scale HCG facility, where near zero axial velocities were seen at 45 jet radii from the center for a downstream location of 100 *D*. Hence a domain width of 55 *D* is large enough such that the influence of radial side walls is minimal. RANS simulations were performed for the smaller domain to justify this fact. The incompressible flow simulation employs wall conditions for the back and side surfaces and an outflow condition at $x = 100\ D$.

The mesh used for the simulation is shown in Figure 4(b). The domain has a total of 16 million cells. As shown in Figure 5, different mesh size is applied in both the axial and radial directions. For the axial direction, a stepwise increasing mesh size is used from the inlet to the location $x = 15\ D$ downstream to make sure that the inner core of the jet is well resolved at entry. In this region the mesh size transitions from *D*/120 to *D*/8 in axial length. For the remainder of the downstream domain ($15\ D < x < 90\ D$), the axial mesh size is *D*/8. The last 10 *D* of the domain in the axial direction is used to form a sponge layer with a mesh size that linearly increases from *D*/8

www.manaraa.com

to $D/2$. To minimize reflection from the outlet boundary of the computational domain, a non-reflecting boundary technique known as a numerical sponge layer is used. This technique is actually a combination of numerical beach and grid expansion to absorb reflective waves coming from the outlet of the computational domain [17] and vastly used in LES studies like B&B and many other recent studies [18, 19]. In the radial direction, a 15 × 15 Cartesian mesh is used at the jet inlet as shown in Figure 4 (b). Each square cell in this Cartesian grid has $D/25\sqrt{2}$ (~0.028 D) size on each side. The very center cell of this grid is collocated with the overall domain centerline, thereby eliminating the need to interpolate for any centerline data for which experimental results are widely available. As can be seen in Figure 4(b) and Figure 5, five radial layers of cells existed between the center of the Cartesian grid and the edge of the circular inlet ($r = D/2$). Outside of this circular inlet, a uniform mesh size is used between $r = D/2$ and $r = D$. The mesh size in this region is similar to the average mesh size contained within the jet diameter. An expanding grid is then used from $r = D$ to $r = 5\ D$. A uniform grid size of $D/8$ is then applied from $r = 5\ D$ to the outside edge of the computational domain ($r = 27.5\ D$). The number of azimuthal divisions is dictated by the 15 × 15 Cartesian array (4 × 15 = 60 divisions). Recent investigations by Kim [15] showed that 60 equal azimuthal divisions is appropriate for LES to capture the flow for a turbulent jet.

www.manaraa.com

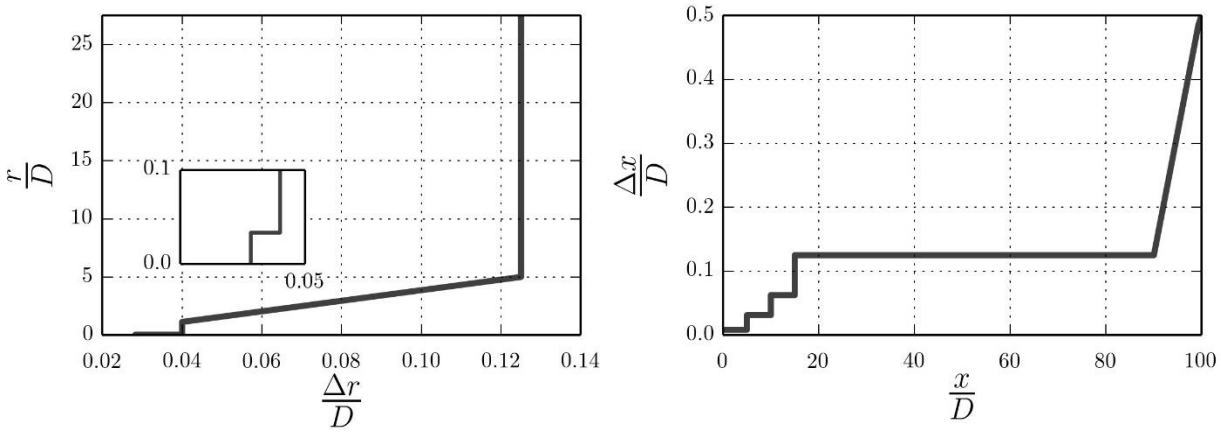

Figure 5. Mesh spacing in radial and axial direction. The grid is symmetric with respect to the jet axis

The open source, finite volume, computational fluid dynamics package, OpenFOAM®, is used for the present study. The selection of the LES Sub-Grid Scale (SGS) model is done by a systematic CFD study. Six different models were compared: 1) Smagorinsky model [20]; 2) Homogeneous dynamic Smagorinsky model [21]; 3) Dynamic local averaged Smagorinsky model [22, 23]; 4) k-equation eddy-viscosity model [24]; 5) Dynamic k-equation eddy-viscosity model [24]; 6) Localized dynamic k-equation eddy-viscosity model. Initial simulations were performed using all the models. Each LES run was initialized with a RANS simulation [25] previously conducted. The incoming flow was assumed to have no fluctuations. A comparison of the simulation results is provided in Figure 6(a), where the inverse of the centerline velocity (U_C) is shown as a function of the downstream distance (x/D). This is often referred to as the decay rate of centerline velocity, and for the results shown, they represent the time-averaged solution from 0 to 6.65×10^2 residence times where residence time for the jets is D/U_{inlet}. For reference, the

www.manaraa.com

stationary hotwire measurements (SHW) from HCG are included along with the RANS results from [25]. From this figure, it is apparent that the simulation which shows the most promise for fast convergence to the measured data is the Dynamic local averaged Smagorinsky model. This SGS model also predicts a smaller potential core length compared to the other models. For these reasons, this model is used within the LES framework for the HCG jet. The model is an implementation of the dynamic Smagorinsky model with coefficients C_D and C_I computed as local average of their face values corresponding to values by Fureby et al [23]. Note that without the effect of inlet fluctuations, the potential core of the jet is incorrectly predicted and does not compare well with the RANS simulations. However, this first phase of numerical explorations provides valuable insight into the different SGS models and their impact on the results.

After adopting the SGS model as described above, the effect of including random fluctuations at the jet nozzle is investigated, with results shown in Figure 6(b), where the centerline velocity is plotted against the downstream distance from the nozzle. From the two LES curves shown, it is easily seen that fluctuating inlet conditions have a large impact on the length of the potential core. For the case with no random fluctuations, even a longer simulation time (0 - 1.33×10^4 residence time) does not decrease the potential core length nearly as much as when those fluctuations are included, even for a short simulation time (0-4.5×10^2 residence time). The fluctuation at the inlet in the simulation is generated using a random fluctuation generator ('turbulentInlet' boundary condition) option in OpenFOAM. The turbulent intensity at the nozzle in the simulation is adjusted to match the reported intensity measurements of 0.58% from the HCG experiments. In the simulation, the potential core length stabilizes within the first 2.5×10^2

www.manaraa.com

residence time. However, even though the turbulent intensity matches at the inlet, it still over-predicts the length of the potential core. Recent LES studies have also predicted a longer potential core length compared to that seen in similar experiments [16, 26]. Literature suggests that the potential core length simulated using LES can vary significantly from measured data and is very sensitive to the inlet flow conditions [15].

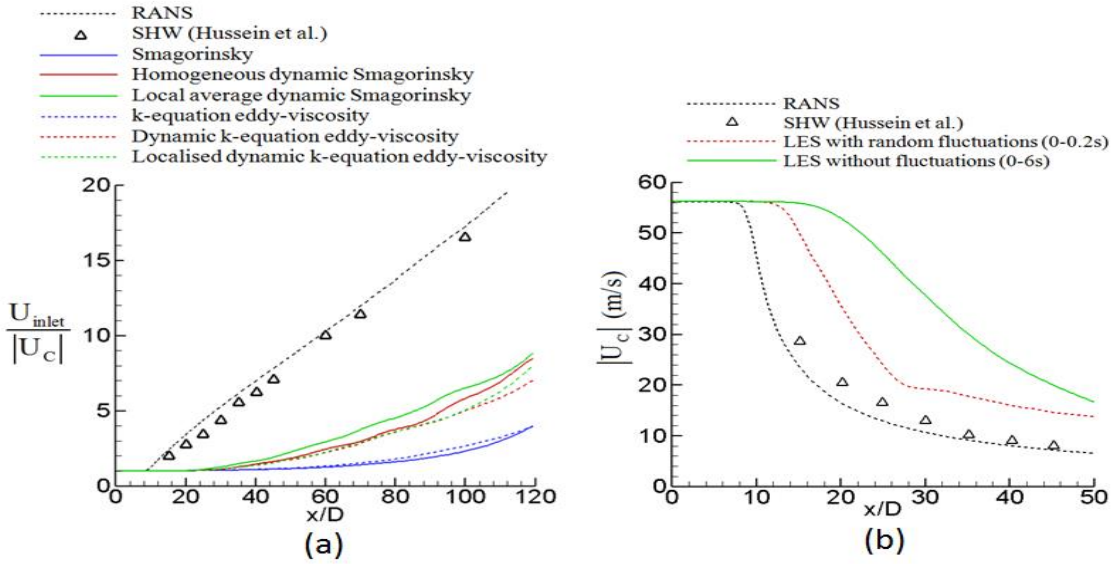

Figure 6. (a) Comparison of mean centerline time averaged velocities for different LES models (|UC| - centerline velocity magnitude; U_{inlet} – average velocity at inlet); (b) The effect of inlet fluctuations on the simulated potential core length.

Multiple factors can govern flow conditions at the jet nozzle [27], and several complicated methods for generating synthetic turbulence exist to address this. However, it is difficult to generate a synthetic turbulence which would exactly give the correct spectrum associated with the turbulence as seen by HCG in their experiments. Hence the most straightforward and accurate approach, albeit computationally expensive, is to perform a precursor simulation of the flow in the

www.manaraa.com

upstream nozzle assembly, completely independent from the LES model of the large enclosure. From this precursor simulation, the fluctuations at the jet nozzle itself can be sampled and transferred to the inlet boundary of the jet simulation.

In their experiments, HCG used two different contractions beginning with a 12 inch duct opening to eventually reach the exit jet diameter of 1 inch which was then directed into the large enclosure previously described. The first upstream contraction was a cubic design and the second was a fifth-order polynomial design. A faithful model for this double contraction is created and shown in Figure 7. Tetrahedral cells were used to mesh the contraction geometry. The model had a total of 0.445 million cells. A very low value of turbulent fluctuation is prescribed at the inlet of the contraction model as would be expected close to the screen mesh of a wind tunnel [27]. Instead of modeling the large enclosure downstream of the nozzle, the flow is directed into a pipe with a diameter twice the size of the jet diameter. This is done in order to reduce computational effort without losing any accuracy in the simulated flow inside the contraction nozzle. The flow inside the contraction domain is first initialized with steady state RANS data. Spalart-Allmaras detached eddy simulation (DES) model was then used to obtain accurate flow conditions at the jet nozzle. The detached eddy model uses RANS equations at regions near solid boundaries thus reducing the computational cell requirement. LES is used for the rest of the domain [28]. Adjustable time stepping is used for the contraction simulation with maximum courant number set at 0.5. As illustrated in Figure 7, transient velocity data is probed and saved at 180 locations (5 equally spaced radial locations at 10° angular increments at the nozzle exit plane).

www.manaraa.com

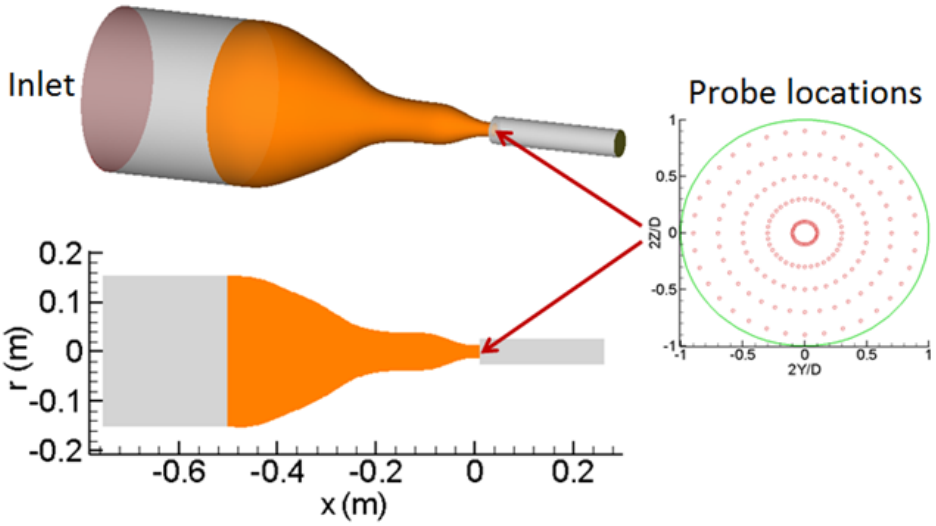

Figure 7. Computational model of the double upstream contraction used in the experiments of HCG

The precursor contraction simulation is performed for a period of 0.18s. The distribution of vorticity magnitude at the nozzle exit at five different time instances is shown in Figure 8. Data during the initial 2.5×10^2 residence time of the simulation is not used. The effect of simulation time on turbulent intensity at the nozzle exit is shown in Table 1. HCG reported unsteadiness of the fan as the major cause of the turbulent intensity at the nozzle exit. Our simulations show that similar turbulent intensity is observed from the flow at the exit of the contraction nozzle without the effect of unsteadiness of the fan. The difference in turbulent intensity calculated using data saved with 90 probed locations and 180 locations was 0.002%. During the period of 0.1-0.18 s, the turbulent intensity is found to be 0.579%, which is nearly identical to the measured 0.58% value reported by HCG. This 0.08 s (0.1-0.18 s) of data from the precursor contraction nozzle simulation in then used as an inlet condition for the isothermal jet simulation for the domain in

www.manaraa.com

Figure 4 and is periodically cycled for the duration of the jet simulation. For example, if the simulation time of the LES domain (refer to Figure 4) is 2 s, this 0.08 s of data is cycled 25 times during that period (2 s/0.08 s = 25). It is interesting to note that the radial component of turbulent intensity is twice that of the axial component at the nozzle exit.

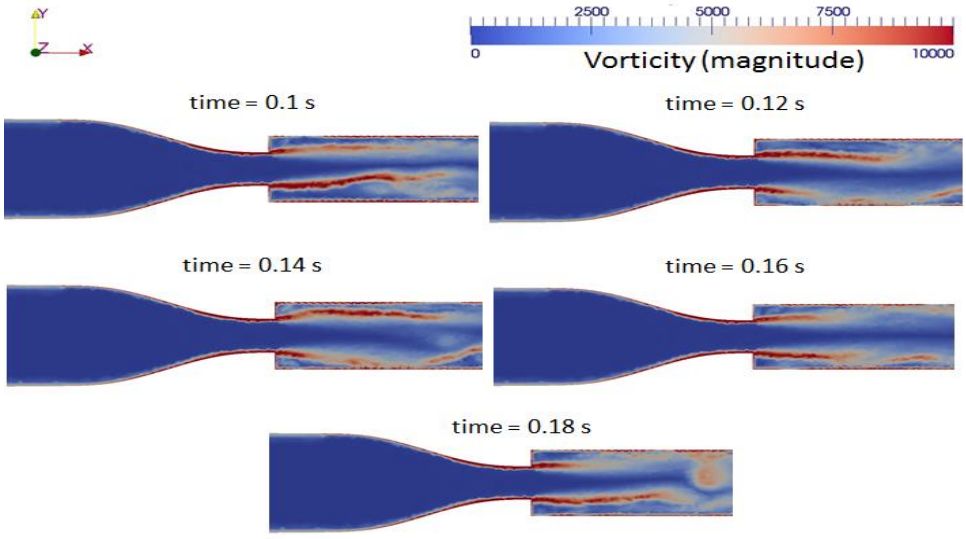

Figure 8. Contours of vorticity magnitude near the nozzle exit at different time instances.

Table 1. The effect of simulation time on turbulent intensity at the nozzle exit

Time interval [s]	*Turbulent Intensity (%)*
0-1 0.12	0.67
0.1-0.14	0.657
0.1-0.16	0.578
0.1-0.18	0.579

www.manaraa.com

With accurate inlet conditions from the precursor nozzle simulation, LES studies of a single, isothermal round jet (Re = 95,000) are performed using the dynamic local averaged Smagorinsky model. Adjustable time stepping with maximum courant number of 0.5 is used for the simulations. Time averaging of the flow quantities is initiated from 3.5×10^2 residence time, i.e. after two cycles of data from the precursor contraction nozzle simulation. 50000 hours of computational effort was used to obtain 2 s (4.4×10^3 residence time) of time averaged LES data.

2.3 RESULTS AND DISCUSSION

2.3.1 Mean velocities and near-field parameters

Figure 9 shows the distribution of vorticity magnitude in the jet at different time steps. With a diameter of 18 *D* and a length of 50.5 *D*, these snapshots display a small section of the entire LES domain. The jet development from the potential core region to a fully turbulent state is presented. The largest Kelvin–Helmholtz rollers of the two mixing layers at the jet edge appear very clearly. These mixing layers develop symmetrically and start breaking down into small scales. Vortical flow structures are originally generated in the shear layers, and then merge at the end of the potential core. Hence a rapid breakdown of the large structures with a growth of the small structures occurs, and the development of the jet becomes asymmetric. The radial spreading of the jet becomes visible just downstream of the potential core. From this figure, it is also apparent that

www.manaraa.com

the flow becomes highly mixed as the jet develops. This is due to the increase in turbulent length scales and/or the sizes of the vertical flow structures further downstream. Although LES captures the large-scale structures, the small-scale features are absent as would be expected. Moreover, the assumption of laminar flow at a large radial distance from the centerline looks appropriate since there is no turbulence manifest in the flows at these locations (very top and bottom edges of images shown in Figure 9).

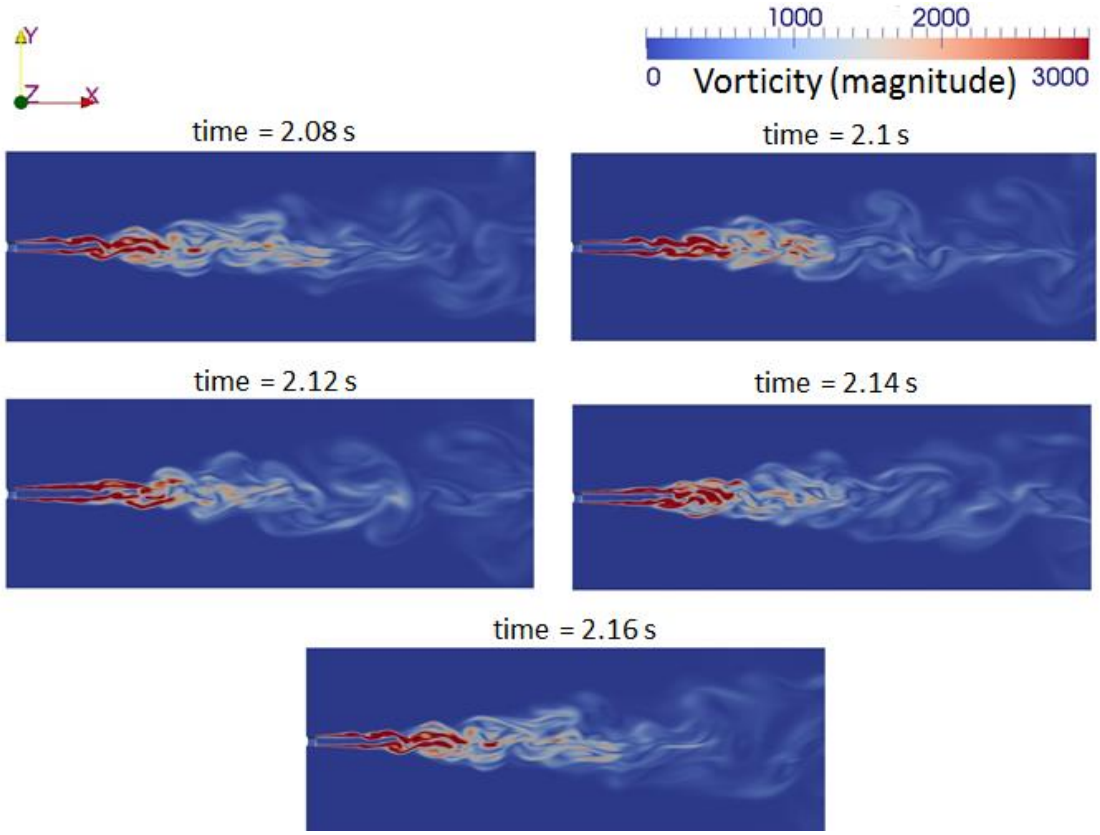

Figure 9. Contours of vorticity magnitude at the nozzle exit for the LES domain at different time instances.

www.manaraa.com

The effect of time-averaging on velocity magnitude is presented in Figure 10. The establishment of a steady state condition is investigated by considering the evolution of centerline velocities. When only averaging between 3.5×10^2 and 1.46×10^3 residence time, the behavior still reveals some time dependence as shown in Figure 10. The time average of the flow reaches its steady value after 3.5×10^3 residence time, evident from the fact that the centerline velocity magnitude remains constant for the remaining three averaging windows included. Also worth noting is that near the inlet, the velocity magnitude of the jet predicted by LES is different from RANS data. This gap is due to the fact that the inlet condition for LES also includes fluctuating components in both the radial and axial directions, while the RANS simulation [25] is initialized with only the turbulence intensity. In reality, the fluctuations present end up contributing to the time averaged downstream velocity component, so this is not entirely unexpected. Figure 10(b) compares the inverse centerline velocity of LES simulation with the measured data from HCG. Plotting the inverse of the velocity data enables better analysis of the low velocity regions sufficiently far downstream of the jet nozzle. This further reveals that with progress of simulation time, the centerline velocity predicted by LES matches the experimental data very precisely. The length of the potential core found by determining the downstream location x, where $u_c(x) = 0.95U_{inlet}$, is found to be 4 D. Although detailed near-field experimental data is not available from HCG, the simulated centerline velocity accurately following the measured data downstream suggests correct prediction of the potential core length. Other LES simulations of jets typically over predict the potential core length. For example, B&B reported 6.5 D, while the experimental data from P&L reported a value of 1.75 D. Also, based on linear fitting of the simulated inverse

www.manaraa.com

centerline velocity between x = 15 and 75 D using time-averaged data from 3.5×10^2 -5.75×10^3 residence time, the virtual origin (x_0) [29] was calculated to be 4 D as was observed by HCG for their measurements. Thus properly accommodating the fluctuating velocities yields results more indicative of the actual flow physics in both the near and far-field, and good agreement can be realized.

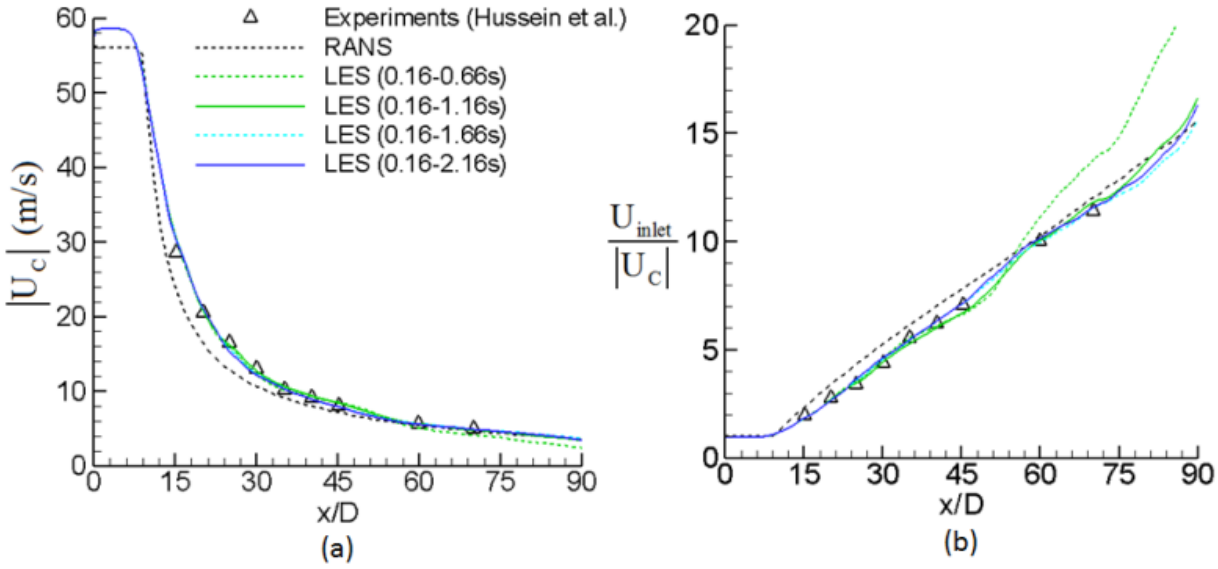

Figure 10. Effect of time-averaging on (a) the centerline velocity magnitude (|Uc|) and (b) inverse centerline velocity for the LES simulation. Data in the initial 3.5×10^2 residence time is not considered in the time-averaging.

2.3.2 Reynolds stresses

In addition to the time averaged velocities within the domain, other key physical quantities are compared to the HCG data. The accurate prediction of the potential core enables the ability to

www.manaraa.com

sample data at the exact locations reported by HCG, namely x = 70 D. Figure 11 (a) shows the time averaged axial stresses for various time intervals at this downstream location. Just as observed for the centerline data, the simulation results approach a time independent solution, such that further averaging would have no impact. The need of azimuthal averaging can be visualized by comparing Figure 11(a) with Figure 11(b). For this reason, data reported for all subsequent plots makes use of azimuthal averaging.

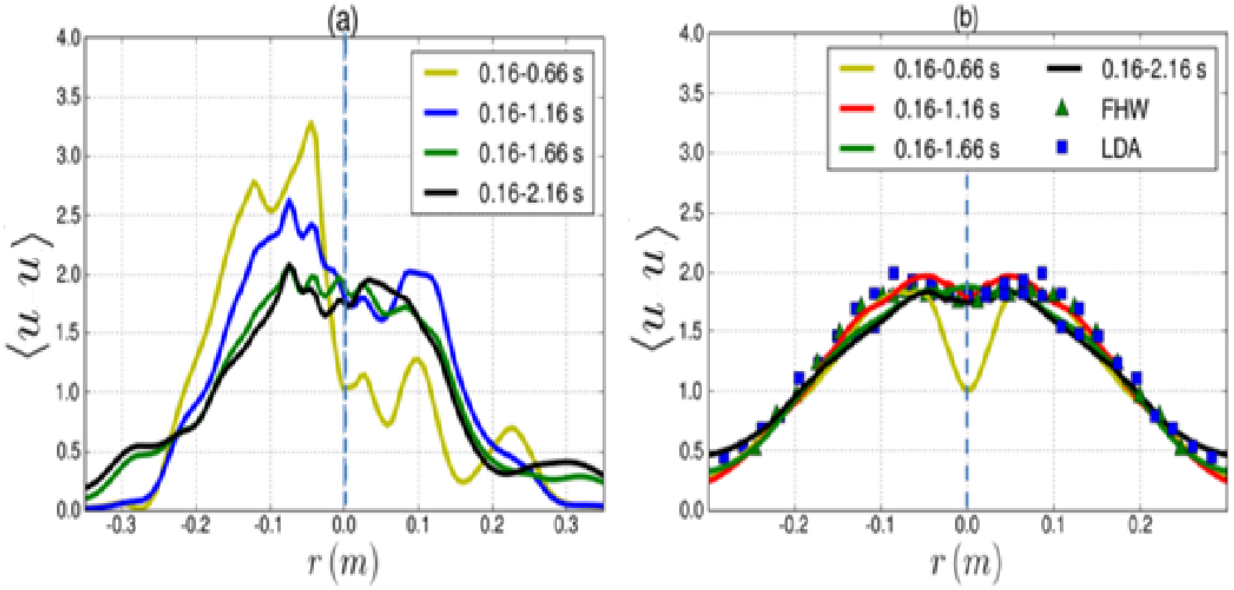

Figure 11. Comparison of axial stress profiles at x = 70 D for different time average interval (a) without azimuthal averaging and (b) with azimuthal averaging. (FHW: Flying Hot Wire measurements LDA: Laser Doppler Anemometer measurements)

As can be seen in Figure 12, LES data also compares very well with the experimental data reported by HCG. The profile of the axial normal stress $\langle uu \rangle$ calculated by LES successfully detects the distinct off-axis peak measured by the LDA/FHW. This peak is consistent with experimental

www.manaraa.com

measurements and is due to the strong off-axis peak in the production of turbulence energy by the Reynolds stress working against the mean shear.

The radial and azimuthal components of Reynolds stresses are presented in Figure 13 and Figure 14 respectively. The radial component near the centerline is very close to LDA measurements of HCG. In addition, the radial stress $\langle vv \rangle$ and azimuthal stress $\langle ww \rangle$ $u'_\theta u'_\theta$closely mimic that from HCG. Figure 15 exhibits turbulent shear stress data $\langle uv \rangle$ $u'_x u'_r$which is consistent with both FHW and LDA data reported by HCG along the radial direction at $x = 70\ D$. The location of the off-axis peak (~0.1 m) for shear stress is close to the radial distance of the same off-axis peak in Reynolds stress as shown in Figure 12.

The Reynolds stresses also exhibit significant anisotropy, which is revealed both by comparing the shear stress shown in Figure 15 and by the difference in the normal stresses (Figure 12, Figure 13 , and Figure 14). On the centerline, the turbulence intensity is about 25% of the mean velocity. Although HCG did not report this number, it can be calculated from their data, and was found to be 24.4%. For this turbulent jet, it is expected to be an axisymmetric flow, a condition that is satisfied when the radial and azimuthal components of turbulent kinetic energy are identical. As can be seen in Figure 13 and Figure 14, this expectation is a valid one.

www.manaraa.com

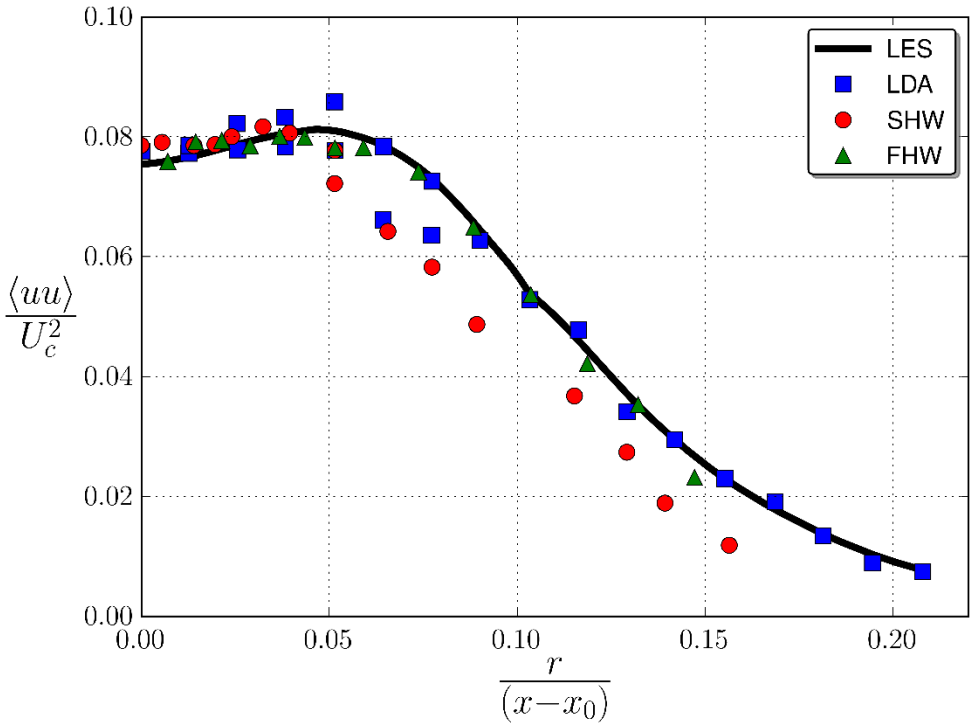

Figure 12. Comparison of axial component of turbulent kinetic energy at *x* = 70 *D*.

www.manaraa.com

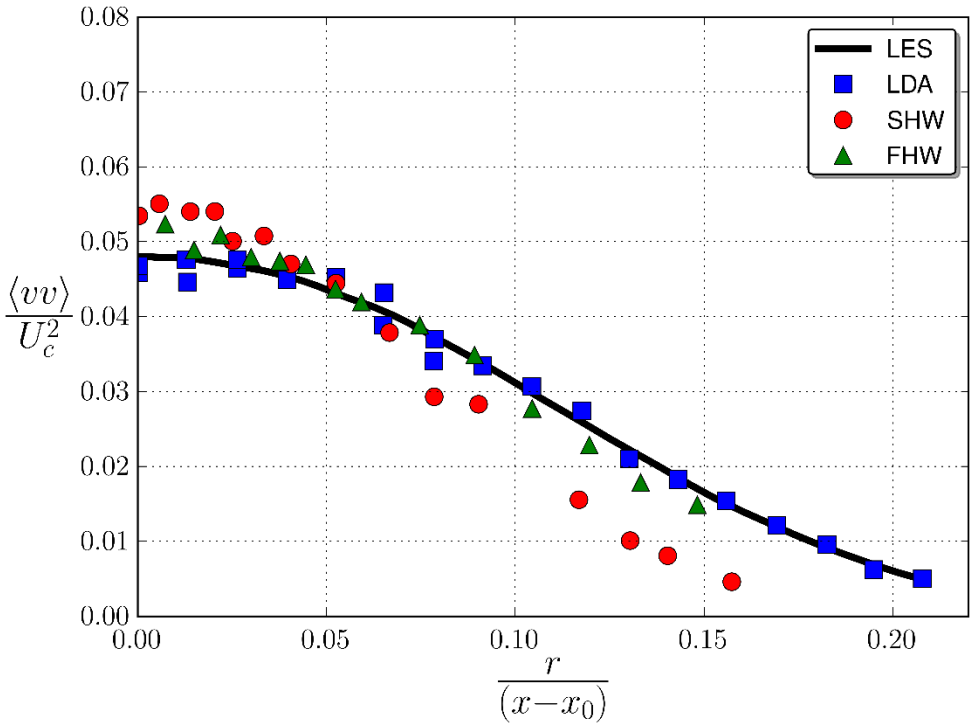

Figure 13. Comparison of radial component of turbulent kinetic energy at *x* = 70 *D*

Another feature worth exploring is the self-similarity of the flow features downstream of the nozzle. The evolution of axial velocity at different axial locations is shown in Figure 16. It shows that axial velocities reveal self-similar behavior in the range of 20 $D < x < 80$ D. Hence for a location where self-similarity is reached, an increase of downstream length of the domain would not provide additional insight. However, it is important to realize that although self-similarity may be reached for the velocities, other quantities like turbulence statistics (e.g., second moments of velocities), might show very different trends in self-similarity. The fact that the same region of self-similarity does not apply for the axial stress component is evident in Figure 17. Close to the

www.manaraa.com

jet nozzle (x = 20 D), the behavior is not consistent with experimental or computational results at x = 70 D. However, these second moments do show self-similar behavior in the range of 50 D < x < 70 D. Therefore the self-similar region can occur at different locations, depending on which flow metrics are of interest.

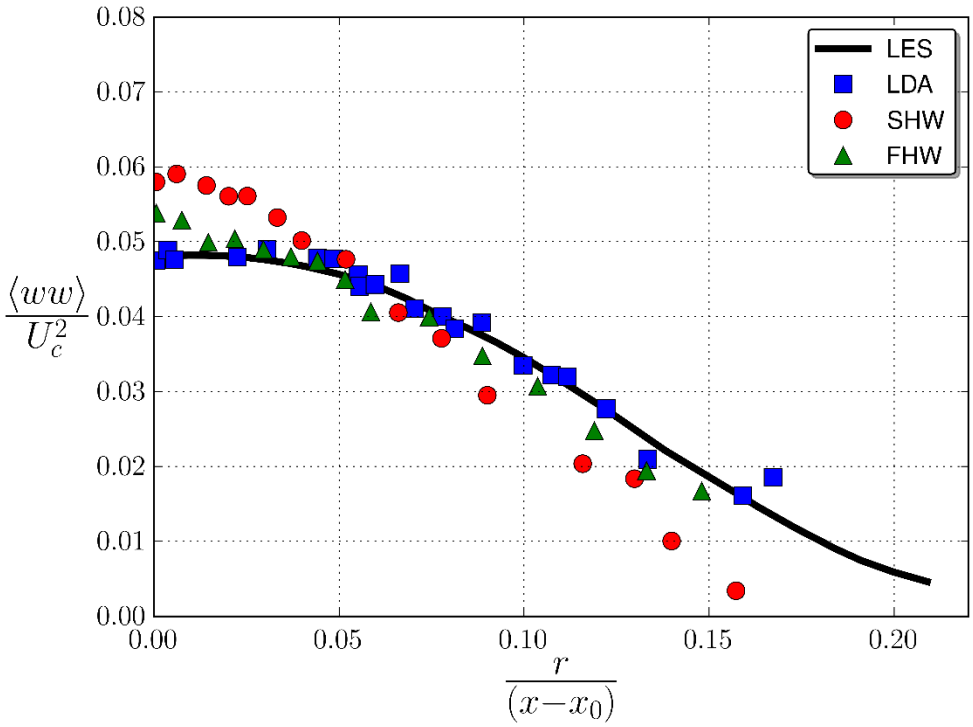

Figure 14. Comparison of azimuthal component of turbulent kinetic energy at x = 70 D

www.manaraa.com

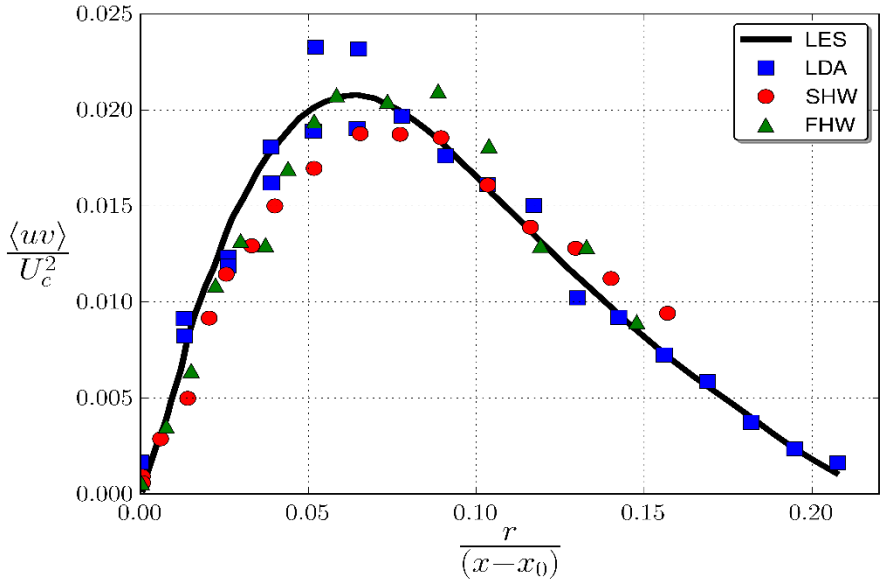

Figure 15. Comparison of turbulence shear stress at *x* = 70 *D*

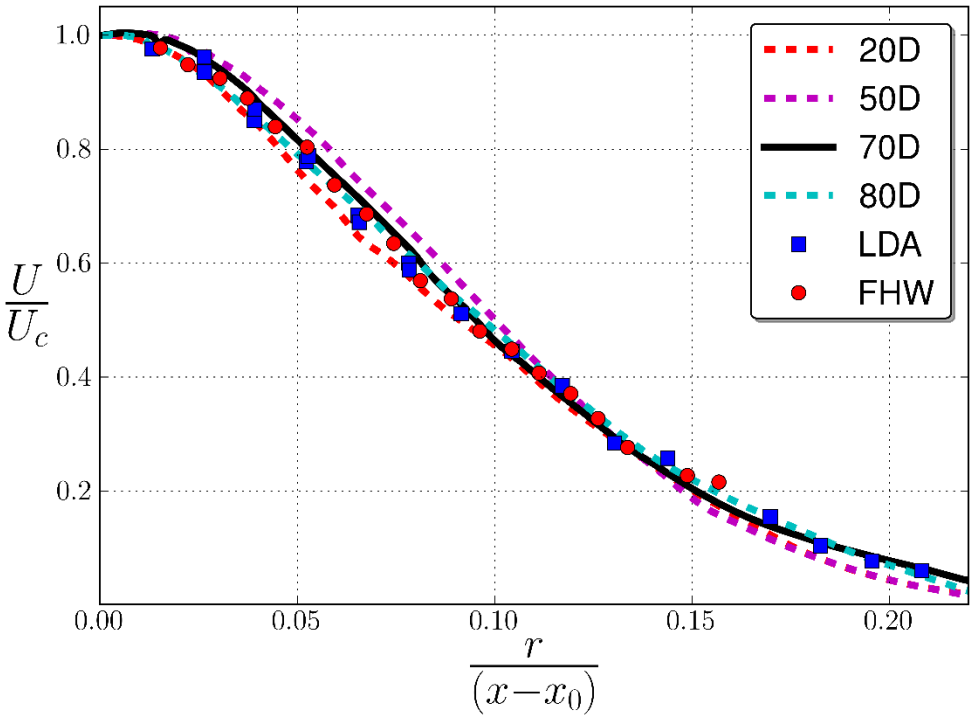

Figure 16. Normalized axial velocity profiles at different axial locations

www.manaraa.com

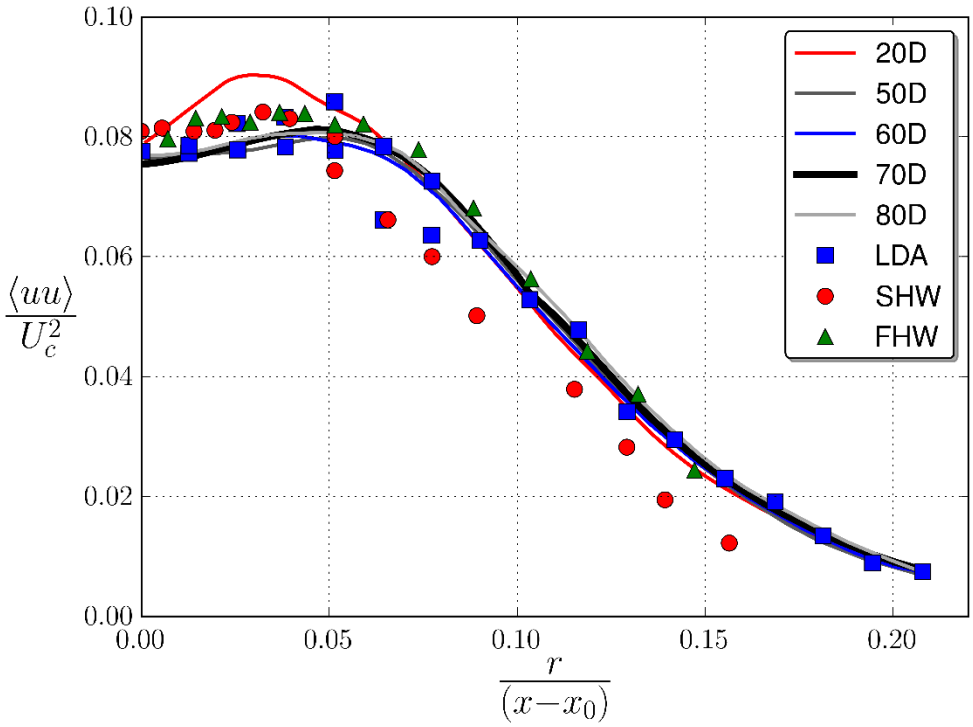

Figure 17. Normalized axial stress profiles at different axial locations

2.3.3 Higher order statistics and budget of turbulent kinetic energy

Due to differences and uncertainties in experimental techniques, full determination of the turbulent energy budget in jets remains difficult to measure. Therefore, in HCG and other previous studies, the authors were unable to experimentally quantify all terms in this budget. In particular, the pressure-velocity correlations or pressure diffusion term is difficult to explicitly define only in terms of measurable quantities. For example, in the jet study by Wygnanski & Fiedler [13], the dissipation term was estimated by assuming semi-isotropic turbulence calculated from the derivatives of the measured velocity fluctuations. This left the pressure diffusion term to be

www.manaraa.com

inferred as the balance of turbulence kinetic energy equation. Similarly, in the axisymmetric jet study of P&L, the pressure diffusion term was neglected altogether and they expressed the energy dissipation term as the closing balance. On the other hand, HCG estimated energy dissipation from experiments with the assumption of locally axisymmetric homogeneous turbulence, and quantified the pressure diffusion as the remaining term. It is important to highlight differences in the data from the two seminal works of P&L and HCG. The TKE budget results represent one such difference. Additionally, there are other slight but important differences that can be seen in reported quantities such as third order moments. When reporting these differences, HCG used this to challenge the accepted dogma regarding the universality of the self-similar region, providing arguments for at least a weak dependency of the far-field upon source conditions. It is important that these and other discrepancies between such highly regarded studies are fully resolved (HCG results for example are considered the best available benchmark for large eddy simulation (LES) validation according to an AGARD report [30]). In particular, attempts are made to settle these differences and confidently attribute them to assumptions previous investigators made or identify key physical differences in the flow given the different Reynolds numbers under investigation. In the current work, two additional LES studies of turbulent free jets are conducted to address these uncertainties. The first LES study is conducted with Re = 10^4 in order to mimic the P&L conditions. The second study employs Re = 2000 in order to resolve any discrepancies due exclusively to Reynolds number (note that with the two additional LES studies, three Reynolds numbers, increasing an order of magnitude in each case are considered). Third order moments of velocities from HCG and P&L are compared to their respective LES studies (hereafter as LES-

www.manaraa.com

HCG and LES-PL). Also, the turbulent kinetic energy budget and the budget of Reynolds stresses are compared with all three values of Re.

2.3.3.1 Profile of triple correlations

The main importance of third order moments is their principal role in the turbulent energy and Reynolds stress budgets. Both slope and magnitudes of the third order moments indirectly appear in those budgets with the potential to greatly affect the flow physics. Therefore, it is important to resolve the inconsistent trends seen in the literature.

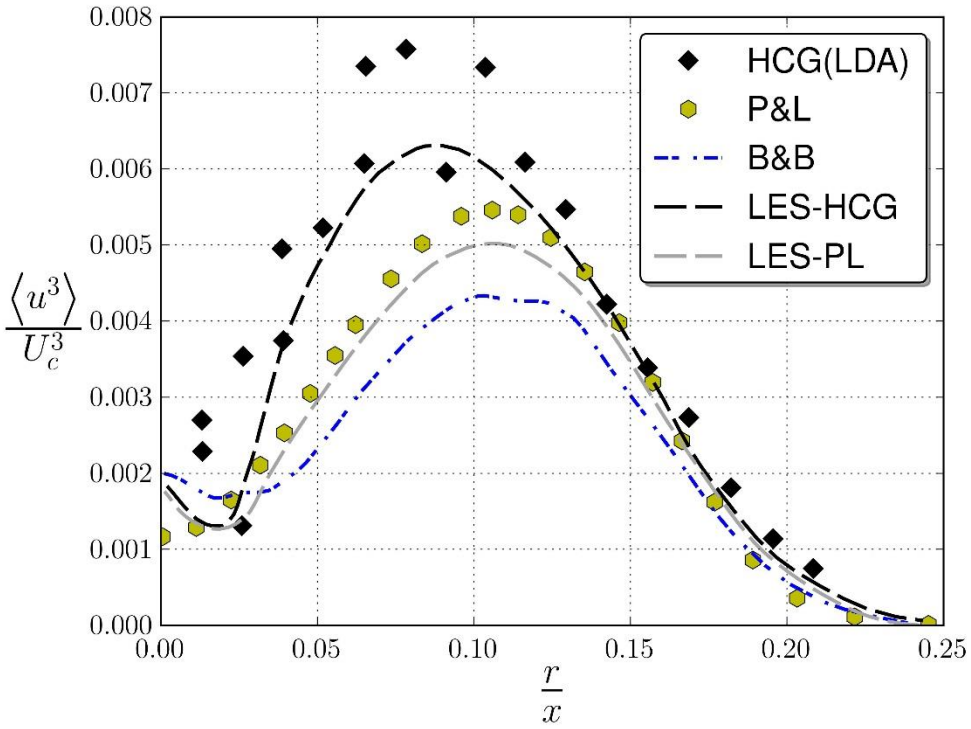

Figure 18. Comparison of axial flux of <uu>

www.manaraa.com

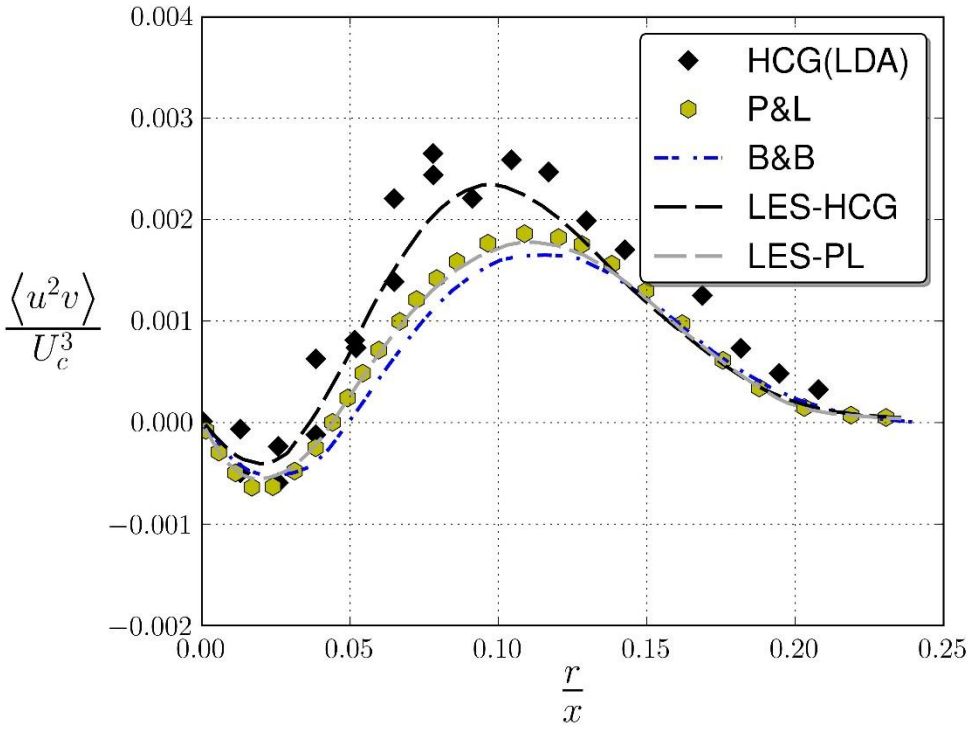

Figure 19. Comparison of axial flux of <uv>

www.manaraa.com

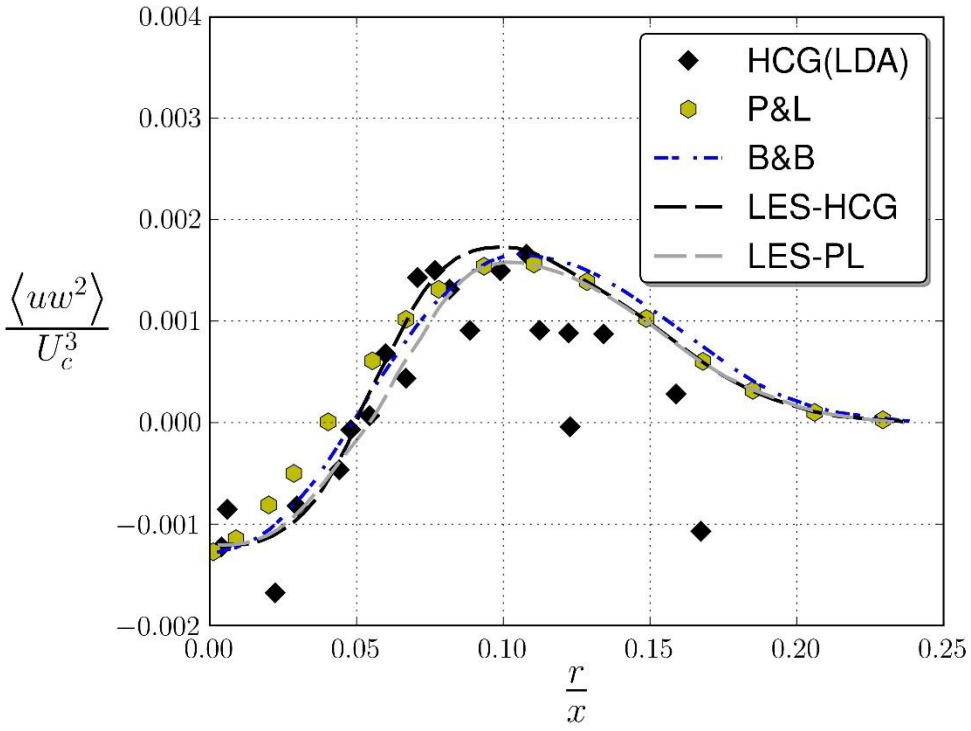

Figure 20. Comparison of axial flux of <ww>

The profile for $\langle u^3 \rangle$ in Figure 18 shows both LES studies have a shape similar to their corresponding experimental curves, but with a lower magnitude. It is should be noted that the LES from B&B, which is also meant to mimic P&L experimental conditions, exhibits this trend as well, but the difference between LES-PL and B&B is coming from the fact that they solved incompressible flow with a compressible solver. The mesh set up and initial condition are also different in B&B compared to LES-PL. Both of these factors play an important role in higher turbulent statistics. Also, near the centerline, both sets of LES data (as well as B&B) show similar trends, namely an initial decrease, followed by an upward trend and subsequent drop after a peak

www.manaraa.com

value is reached. Figure 19, Figure 20 and Figure 21 show negative values near the centerline, which according to P&L, has an important influence on the turbulent transport of the jets. Although all three figures exhibit similar shape experimentally and computationally, magnitude and in some cases peak locations differ in Figure 19 and Figure 21. Moreover, all the LES results are in agreement with P&L in $\langle uw^2 \rangle$ in Figure 20 rather than LDA measurements of HCG, which appear to be extremely noisy. This noisy behavior is to be expected since very high turbulent intensity was observed away from the core region of the jet (the explanation offered by HCG). The LES-PL results show a very good agreement with P&L data in these three mentioned figures, but, near centerline for $\langle uv^2 \rangle$ it has a smaller magnitude similar to that of B&B and HCG results (see Figure 21). The LES-HCG data, on the other hand, have similar maximum location as HCG data, but far from centerline they follow trends common to P&L data. Figure 22 clearly displays each LES result and their corresponding experimental data for $\langle v^3 \rangle$. Here, LES-PL shows a similar shape to B&B but both have higher magnitude in comparison with experimental data of P&L, particularly around the peak location. The LES-HCG again follows HCG trend wise, but with a slightly lower magnitude.

For the $\langle vw^2 \rangle$ trends shown in Figure 23 (where no experimental data is available), it is worth noting the magnitude is around half of the $\langle v^3 \rangle$ data shown in Figure 22. With this result, the common approximation of both HCG and P&L, $\langle v^3 \rangle = \langle vw^2 \rangle$ seem very questionable. This approximation is used in both experimental studies to evaluate turbulence diffusion terms due to difficulty of acquiring through actual measurements.

www.manaraa.com

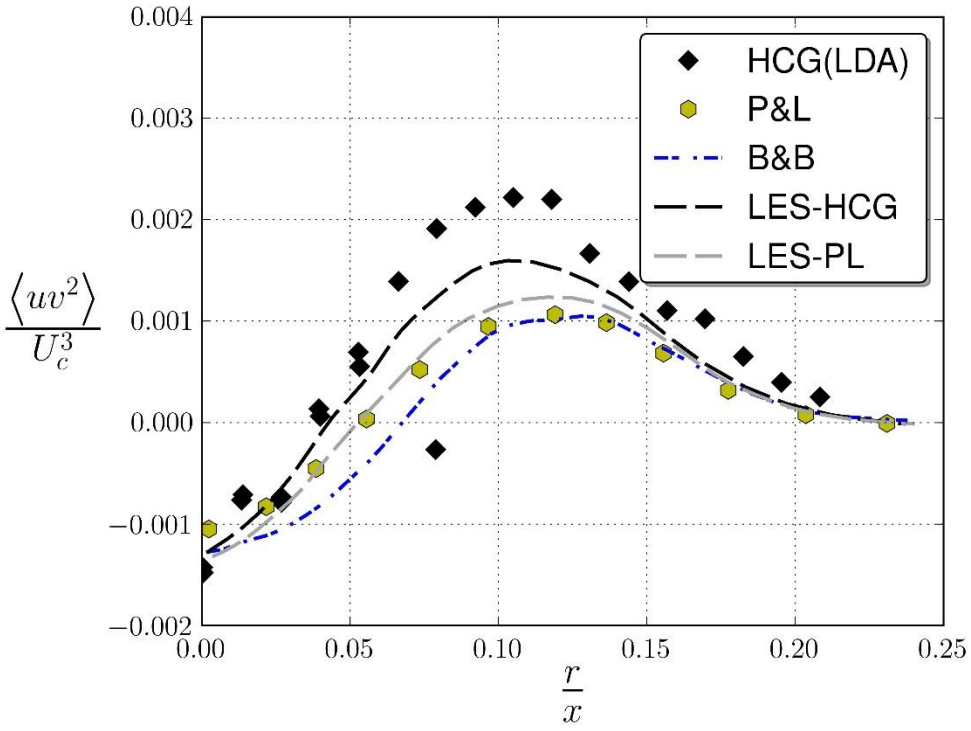

Figure 21. Comparison of radial flux of <uv>

www.manaraa.com

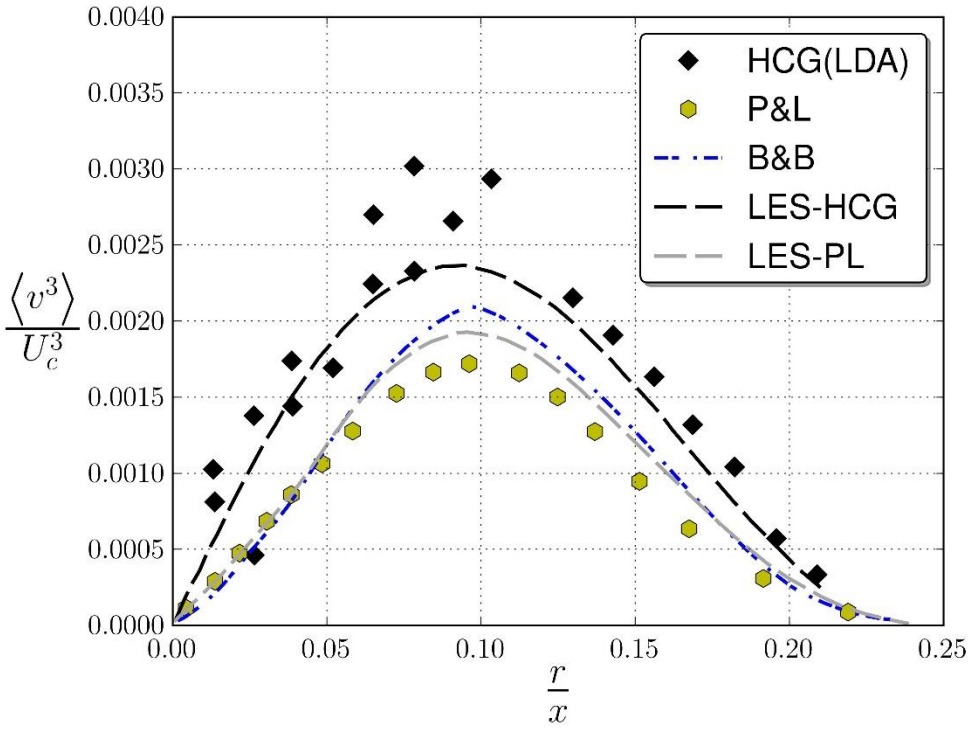

Figure 22. Comparison of radial flux of <vv>

www.manaraa.com

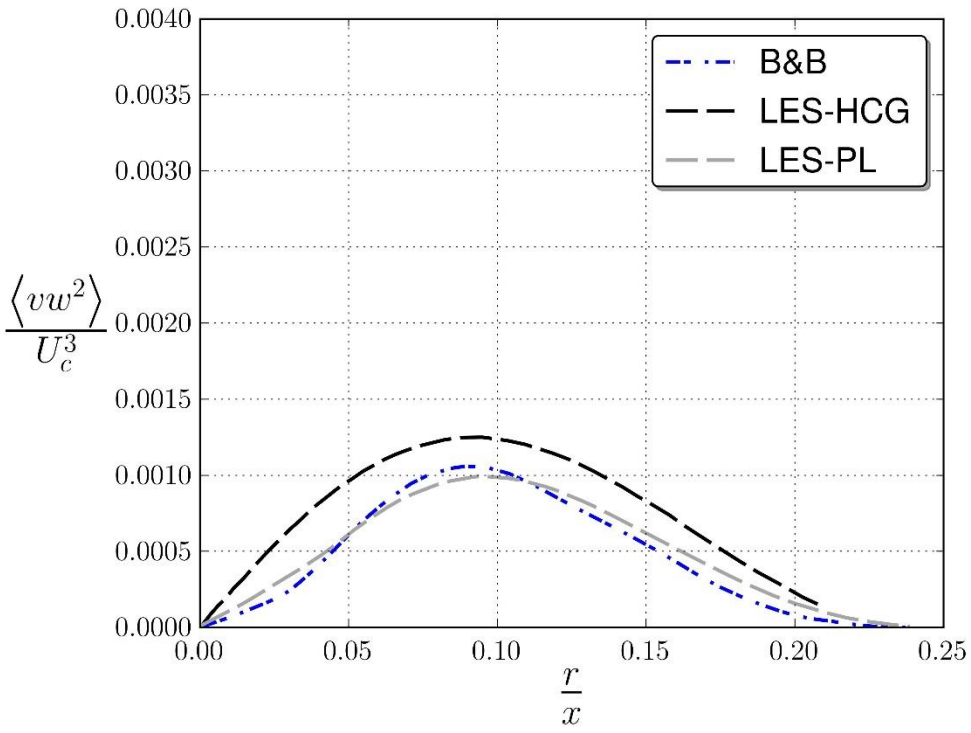

Figure 23. Comparison of radial flux of <ww>

2.3.3.2 Turbulent kinetic energy budget

The turbulent kinetic energy budget is one of the physically descriptive criteria to assess evolution of a turbulent jet flow. This budget, by which the contribution and balance of different mechanisms such as convection, dissipation, diffusion and production can be assessed, provides valuable insight into the physics of the turbulent jet. The measurement of the turbulent kinetic energy budget of the jet has been a topic of large interest in several previous studies, both of an experimental and computational nature, including HCG, P&L and B&B. To address some serious discrepancies regarding the turbulent kinetic energy budget in the aforementioned studies, this is

www.manaraa.com

now investigated in greater detail. In addition to the two Reynolds numbers considered for duplicating HCG and P&L studies, another LES study is included with Reynolds number of Re = 2000 (hereafter as LES-2000), which corresponds to a recent DNS study by Taub et al. [31] .

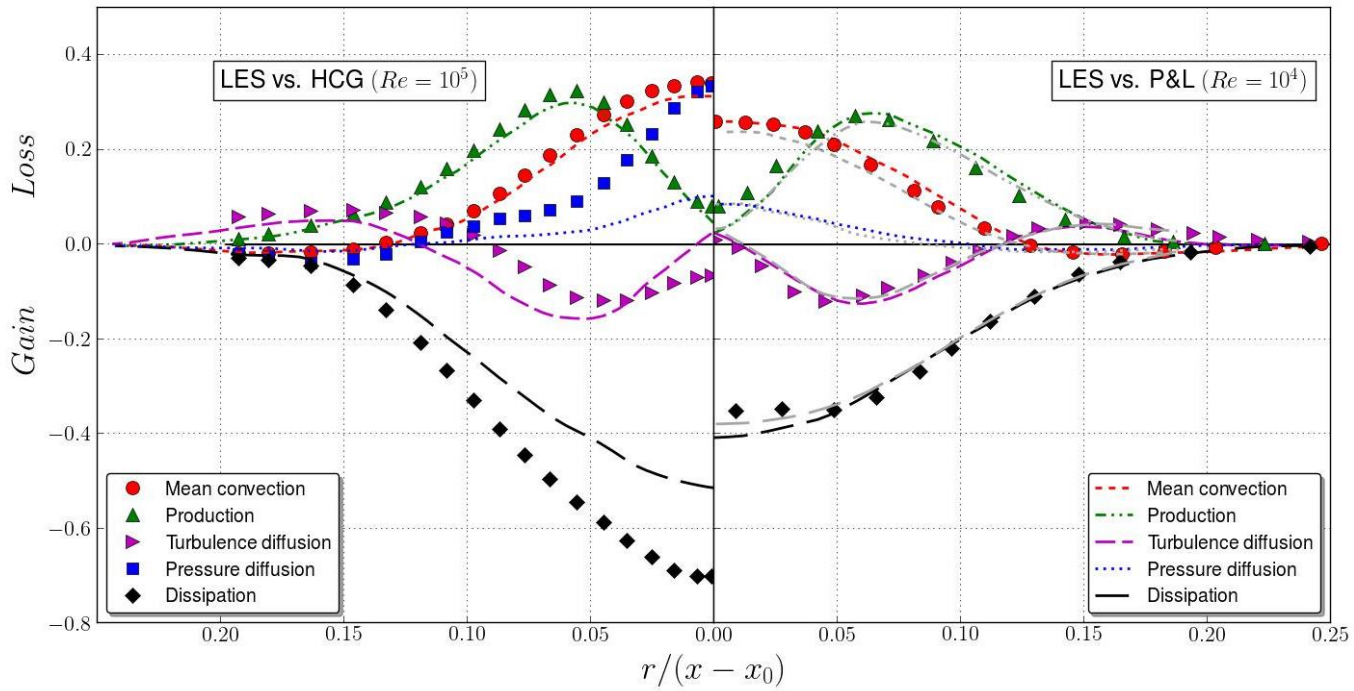

Figure 24. Turbulent kinetic energy budget in self-similar region, quantities are normalized by $\langle U_c^3 \rangle$. Grey lines corresponding to LES data of B&B.

The budget for the turbulent kinetic energy in the self-similarity region of the jet is presented in Figure 24 for the Re = 10^5 (same as HCG) and Re = 10^4 (same as P&L) on the left and right sides of the figure, respectively. Note that for the Re = 10^4 case, the B&B LES results are also provided for comparison. The LES reported values are calculated explicitly from the LES data without any assumptions similar to those adopted by HCG and P&L. LES-PL reveals a very

www.manaraa.com

good agreement with both P&L and B&B for the mean convection, production, dissipation and turbulence diffusion. However, P&L neglected the pressure diffusion term altogether, and quantified dissipation as the balance after accounting for all the other terms. This assumption by P&L of neglecting the pressure diffusion term seems unsubstantiated given the non-negligible magnitude of the current LES results, which are also consistent with the LES from B&B.

The LES-HCG results (left side of Figure 24), find very good agreement for mean convection and production, but cast serious doubt on assumptions used by HCG to calculate pressure diffusion and dissipation. In the HCG study, dissipation was evaluated by a mathematical model called *axisymmetric turbulence* which results in a higher magnitude for dissipation in comparison to the LES results as well as measurements from P&L. Consequently, evaluation of pressure diffusion as the closing term of the energy budget appears to have magnified the difference between both LES and P&L data compared with the HCG measurement of the pressure diffusion term. In reality, the pressure diffusion profiles are similar for both HCG and P&L. Turbulence diffusion of LES-HCG, on the other hand, follows a similar trend as P&L and B&B particularly near the centerline, which is not consistent with the experimental results of HCG. It is coming from the fact that HCG could not capture negative values near centerline for those mentioned triple correlations which determine turbulence diffusion.

www.manaraa.com

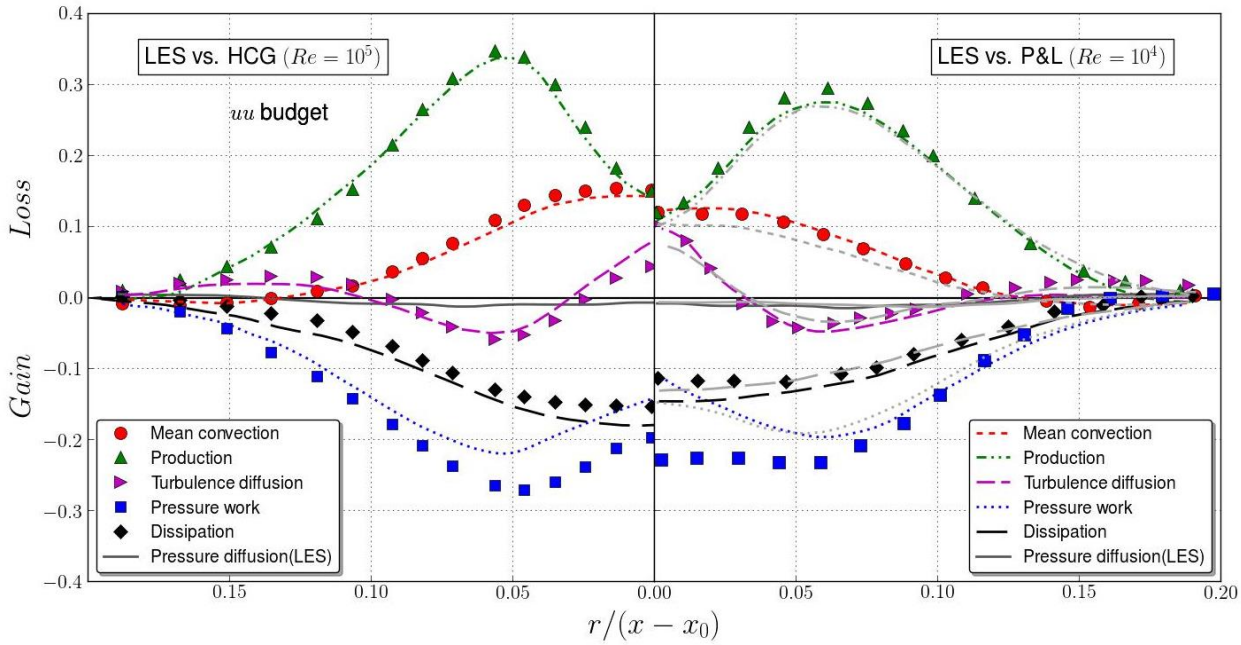

Figure 25. Balance of <uu> in self-similar region, quantities are normalized by $<U_c^3>$. Grey lines corresponding to LES data of B&B

www.manaraa.com

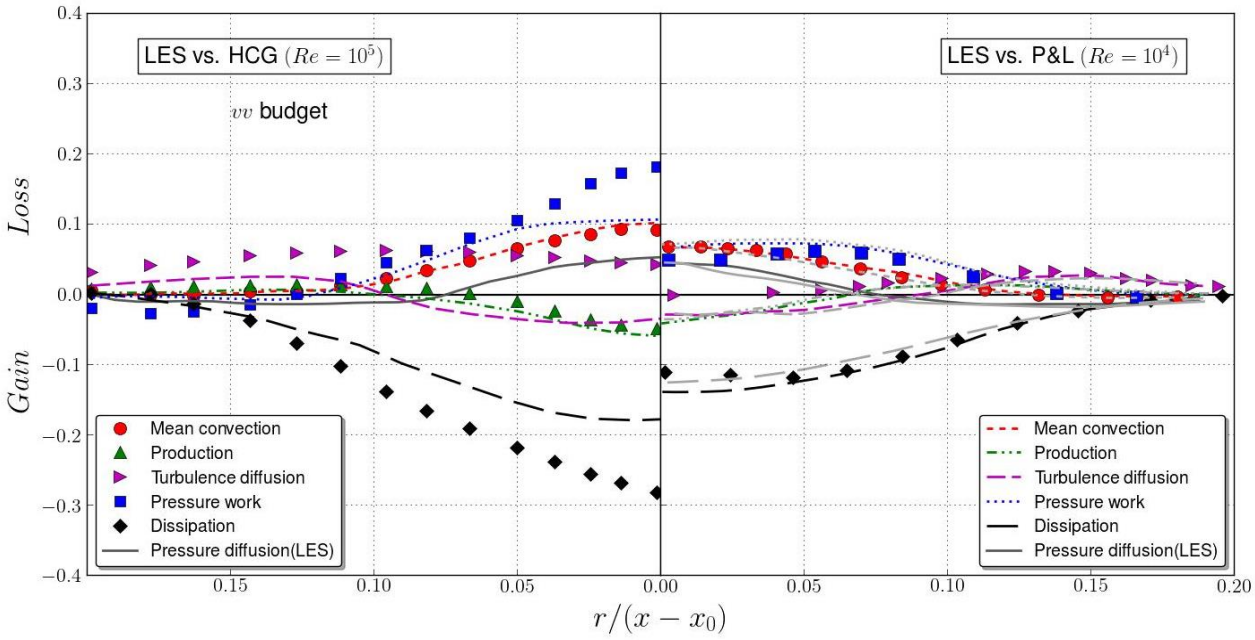

Figure 26. Balance of <vv> in self-similar region, quantities are normalized by $<U_c^3>$. Grey lines corresponding to LES data of B&B

www.manaraa.com

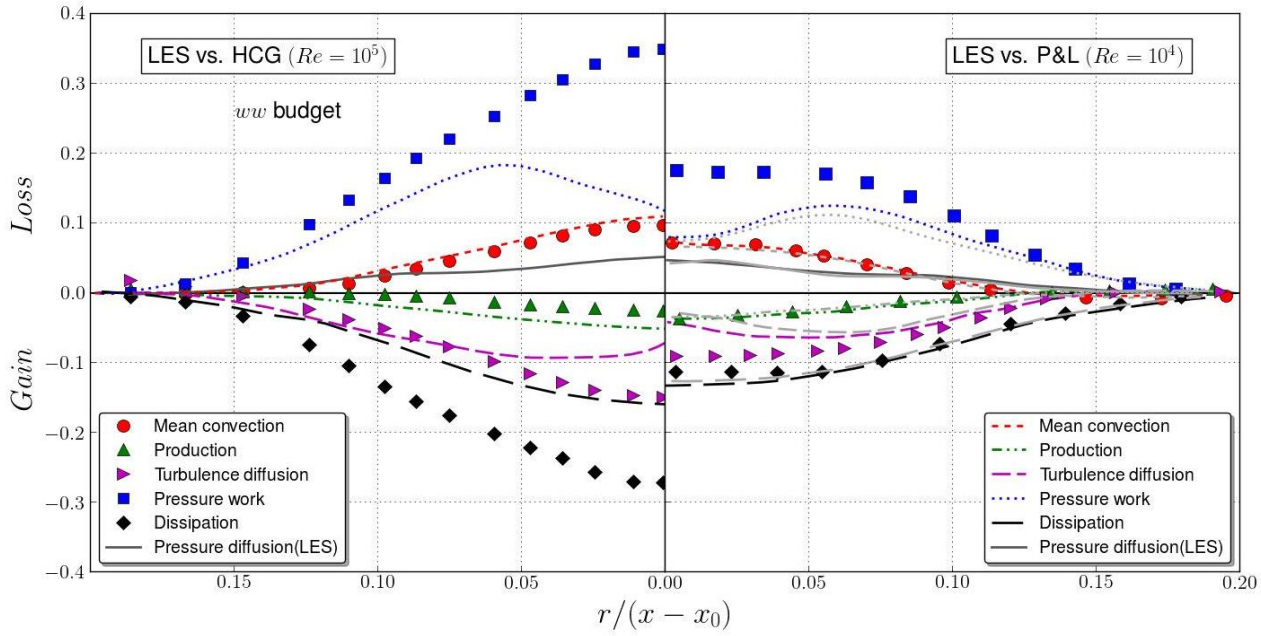

Figure 27. Balance of <ww> in self-similar region, quantities are normalized by $<U_c^3>$. Grey lines corresponding to LES data of B&B

To examine the role of the different mechanisms in the turbulent kinetic energy within the jet, the budgets for the three energy components <uu>, <vv> and <ww> of LES-HCG and LES-PL are presented in Figure 25, Figure 26 and Figure 27. They are compared with the energy component budgets obtained by HCG, P&L and B&B. To evaluate these components, P&L neglected the pressure diffusion and also assumed small scale isotropy for the dissipation components and finally evaluated the remaining pressure terms as the balance. HCG, instead, again used the axisymmetric dissipation assumption and solved the closing balance as pressure work. Both HCG and P&L assumed $<vw^2> = <v^3>$ for turbulence diffusion calculation.

www.manaraa.com

For the three energy components, there is a good agreement between the LES-PL and P&L terms related to mean convection, production and dissipation. This agreement supports the assumption of isotropic dissipation made by P&L. As mentioned in the B&B paper, the difference between turbulence diffusion terms in radial and azimuthal components are coming from the assumption of $\langle vw^2 \rangle = \langle v^3 \rangle$ in P&L and HCG for calculation of turbulence diffusion. This discrepancy of turbulence diffusion near the centerline which is trivial in the radial component and significant for the azimuthal component, indirectly affects pressure work terms. Similar behavior is observed for the HCG measurement of pressure work. In the radial component also, P&L reported zero production, while all the LES calculations and data of HCG measurements show small, but negative magnitude near the centerline which rapidly goes to zero toward the outer radius of jet. The effect of the dissipation assumption of HCG both on the dissipation itself and indirectly on pressure work terms can be seen by comparing LES-HCG data with P&L and B&B.

The budget of the Reynolds stress is lastly presented in Figure 28. Both the LES data agree well with their corresponding experimental measurements, but the effect of Reynolds number on production and pressure work is much more obvious in this figure. Mean convection and turbulence diffusion terms of Reynolds stress budget seem identical both experimentally and computationally in both Reynolds number studies.

www.manaraa.com

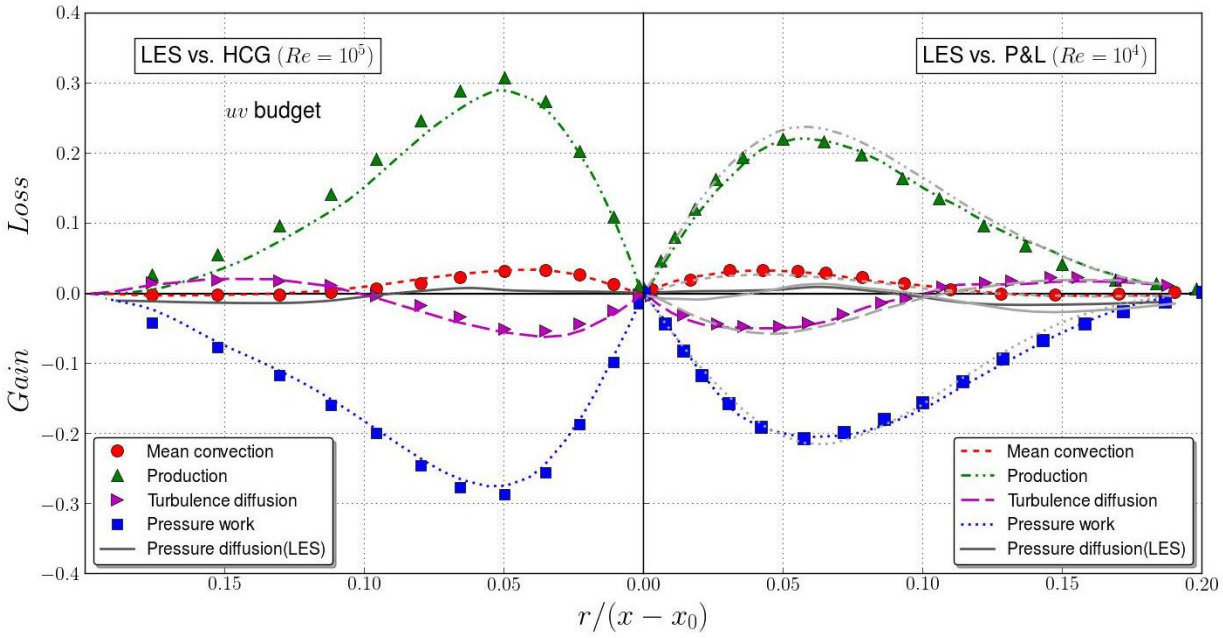

Figure 28. Balance of <uv> in self-similar region, quantities are normalized by $<U_c^3>$. Grey lines corresponding to LES data of B&B

With the purpose of clarifying the differences between the data from two Reynolds numbers which differ by an order of magnitude, particularly in terms like mean convection and production which can be measured reliably [31], the LES-2000 study is conducted. Together, these three simulations provide the perspective needed to accurately quantify the budget for turbulent kinetic energy through comparison with the two benchmark experiments of HCG and P&L (along with the corresponding LES from B&B) and the DNS study of Taub et al. [31] The accommodated Reynolds numbers for this comparison are 10^5, 10^4 and 2000 for LES-HCG, LES-PL and LES-2000, respectively. The results are shown in Figure 29 and Figure 30. Both LES and experimental results show that magnitude and peak location of mean convection and production terms vary with

www.manaraa.com

Reynolds number, while this dependency is negligible in pressure diffusion results of LES. Turbulence diffusion also reflects a Reynolds number dependence on both magnitude and maximum locations.

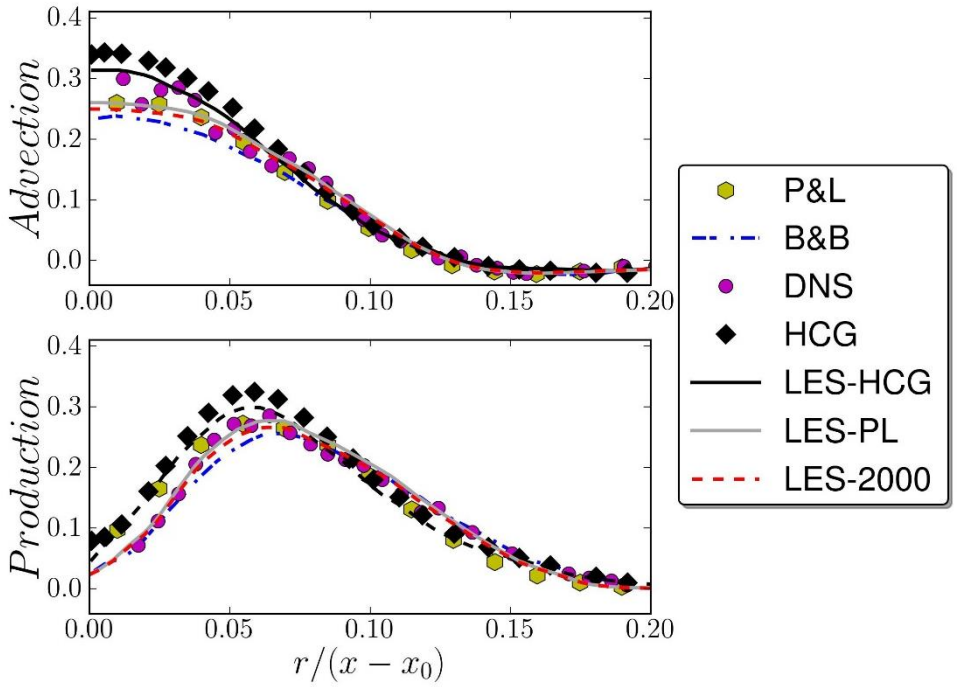

Figure 29. Comparison of mean convection (advection) and production of turbulent kinetic energy budget in self-similar region, quantities are normalized by $\langle U_c^3 \rangle$.

The difference between LES-HCG and LES-PL is larger than the gap from LES-PL to LES-2000, so the dependency on Reynolds number appears to be higher as Reynolds number increases. The location of peak in diffusion terms vary significantly with Reynolds number in comparison with other terms. As shown in Figure 30, peak locations of diffusion terms move to further downstream location as the Reynolds number grows. In general, each jet can be

www.manaraa.com

characterized by its Reynolds number in terms of higher turbulent statistics and turbulent energy budget.

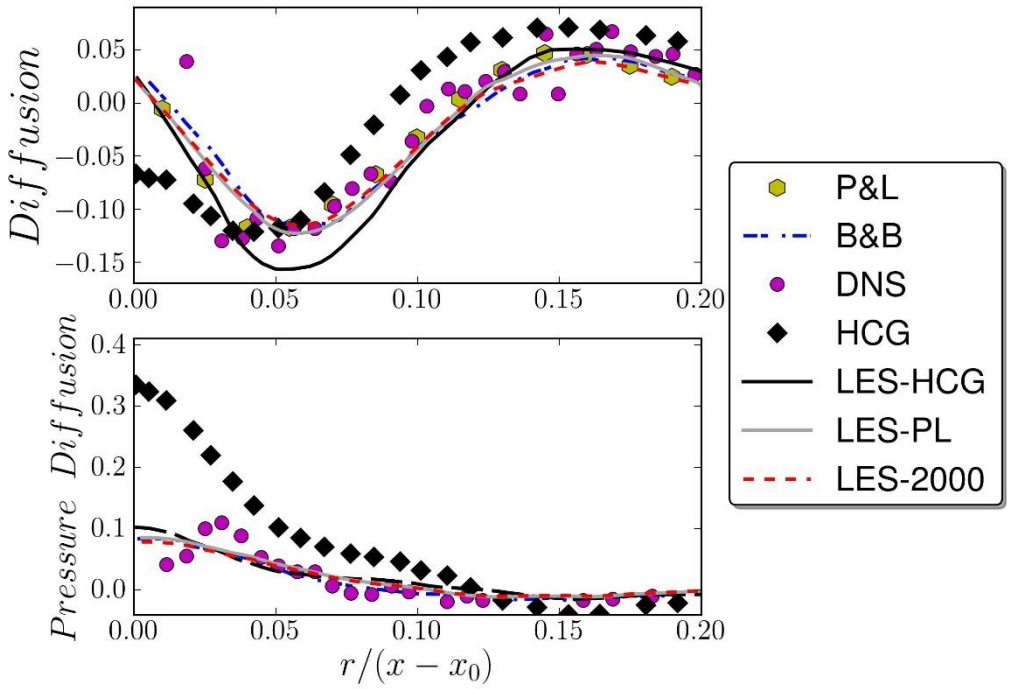

Figure 30. Comparison of turbulence diffusion and pressure diffusion of turbulent kinetic energy budget in self-similar region, quantities are normalized by $\langle U_c^3 \rangle$.

2.4 CONCLUSION

In summary, LES studies of turbulent jets between Re = 2000 and Re = 10^5 have been conducted. This has enabled characterization of turbulence properties of a round jet by its turbulence statistics and the budget for turbulent kinetic energy and each of its components. The

www.manaraa.com

directly obtained flow statistics from these LES studies have been compared to experimental data of HCG and P&L.

The LES results have shown that the approximation regarding $\langle vw^2 \rangle = \langle v^3 \rangle$ made by both HCG and P&L is inaccurate. Turbulence diffusion has also been found to be trivial in the budget of turbulent kinetic energy, which is in agreement with P&L, but casts doubt on turbulence diffusion and hence, dissipation calculations. The effect of Reynolds number on turbulence statistics, particularly on third order moments and the energy budget, have been studied. Terms like mean convection and production are found to be influenced by Reynolds number and inlet conditions.

Hence, for the complex geometries with a range of jet Reynolds numbers like the HGTR lower plenum, this study emphasizes the significance of both Reynolds number and the upstream flow conditioning. Even though this LES work has been computationally costly, it provides key insights into the physics tied to an isothermal turbulent round jet. This critical first step greater enables the development of a trusted approach to eventually modeling the HTGR lower plenum. It is important to note that having such highly detailed experimental results like HCG and P&L has greatly aided the computational simulation in different stages of this study. The more statistics available, the more useful they are in terms of validating a computational model. In general, the luxury of experimental data does not always exist, which is where V&V becomes even more important, especially in the simulation of complex geometries and physics, which is the case for the HTGR lower plenum. The high fidelity results are also due in part to the fact that HCG provided

www.manaraa.com

detailed measurements of the upstream flow conditioning components. Without such details, the modeler is forced to fill in the gaps, which in some cases creates otherwise non-existent problems.

This chapter outlines a detailed isothermal LES study. Additional flow configurations include flow past a cylinder (both isothermal and non-isothermal) and non-isothermal jet flow, which are now considered in Chapters 3 and 4, respectively.

www.manaraa.com

3.0 LARGE EDDY SIMULATION OF NON-ISOTHERMAL TURBULENT FLOW PAST A CIRCULAR CYLINDER

Understanding the thermal mixing of coolant jets in the lower plenum of High Temperature Gas-Cooled Reactors (HTGR) is very important to address certain design and safety issues. As a step towards developing an experimentally validated computational model for the lower plenum flow, turbulent flow and heat transfer around a circular cylinder is computed using large eddy simulation (LES) at three different Reynolds numbers (3000, 5900, 7400). In the range of the Reynolds number considered in this study, flow undergoes a rapid structural change with Reynolds number which significantly affects the heat transfer characteristics. The major difficulty of predicting turbulent heat transfer around a circular cylinder comes from turbulence modeling. To overcome this issue, a finite-volume solver with compressible flow formulations are used for the simulation. A sub-grid stress (SGS) model is chosen in such a way that LES can predict the physical characteristics of the flow and heat transfer. The LES results are found to be in good agreement with well-known experimental studies available in the literature. The main features of turbulent heat transfer in the subcritical regime are closely captured by LES, namely the thermal boundary layer and the sharp increase in both the mean and the r.m.s. Nusselt number in the separation region. The dependence of these quantities on Reynolds number is also captured. The numerical results also confirm that the heat transfer characteristics are closely consistent with the structural change in the flow and is dependent on the Reynolds number. This chapter lays the groundwork needed to develop a high-fidelity experimentally validated computational model of the complex thermal mixing around cylindrical posts in the HTGR lower plenum.

www.manaraa.com

3.1 INTRODUCTION

The goal in this chapter is to computationally model non-isothermal flow past a cylinder as a fundamental benchmark in order to better quantify the physics behind thermal striping in the lower plenum. Detailed analysis will also provide the insight required to potentially modify the reactor design itself, and help establish regulations for HTGRs.

In the range of Reynolds number which we focus on in this study, a laminar boundary layer is formed at the stagnation point of the cylinder, and then separates from the cylinder surface and forms a shear layer which eventually establishes the wake downstream of the cylinder. In this subcritical regime, the Kelvin-Helmholtz instability along with the Karman vortex-shedding cause the separated shear layer to become unstable. As the Reynolds number increases in this range, the flow structure changes very fast, and the mixing of momentum as well as scalar mixing increase with this change. Consequently, heat transfer characteristics follow this change in flow structure, and sees large improvement at the cylinder surface in the separated region.

Several experimental attempts have been made to investigate the unsteady heat transfer in the separated flow region of the cylinder. This investigation of unsteady heat transfer is very important to clarify since it aids in understanding the flow characteristics close to the cylinder body. Scholten and Murray [32] measured the unsteady heat transfer for a range of Reynolds numbers from 7000 to 50,000 while Nakamura and Igarashi also made several attempts to report measurements for a wide range of Reynolds numbers [33, 34]. Among those attempts, Nakamura and Igarashi [34] experimentally investigated unsteady heat transfer from a circular cylinder in a

www.manaraa.com

cross-flow of air for Reynolds numbers between 3000 and 15,000. They measured fluctuating heat transfer on the cylinder surface using a heat flux sensor, and also measured time-spatial characteristics of the heat transfer by an infrared thermograph. Their circular cylinder had a diameter of d = 50 mm and a length of L = 150 mm, which was set horizontally in a wind tunnel. The surface condition of the cylinder was a constant wall temperature and the temperature difference between the cylinder surface and the upstream flow was approximately 25°C. In the current study, this setup is computationally mimicked.

In spite of experimental attempts, surprisingly the reported computational simulation of the flow phenomena is limited in the literature. One major hurdle in simulating turbulent heat transfer around a circular cylinder stems from turbulence modeling deficiencies. Obviously, Reynolds-averaging is not capable to handle the real physics of a non-isothermal flow over a cylinder due to the laminar-turbulent transition as well as the active presence of both thermal and velocity fluctuations. Large eddy simulation (LES) is a more feasible approach, since the large scale structures are solved directly and the effect of small scales are modeled by an appropriate SGS (subgrid stress) model. Plenty of isothermal LES studies of flow around a circular cylinder exist in literature (see [18, 35, 36] for example), but for non-isothermal flow around a cylinder, only a single LES study can be found. Kim et al. [37] considered both the flow and the heat transfer in their LES study. They carried out LES of turbulence flow and heat transfer around circular cylinder in cross flow for three subcritical Reynolds number of 3900, 10,000 and 18,900 using Fluent. Although their LES predictions were in good agreement with the experimental data of Nakamura and Iragashi [34], their results in both the mean and the r.m.s. Nusselt number show undesired

www.manaraa.com

deviation from the experimental results. The work presented here uses an appropriate SGS model and adequate domain size to provide direct validation using the experimental measurements of Nakamura and Iragashi [34].

3.2 LES SIMULATION OF ISOTHERMAL FLOW OVER A CYLINDER

In order to provide an indication of accuracy and capability of the OpenFOAM toolbox for performing LES of flow over a cylinder, a 3D LES simulation of isothermal flow over a cylinder at Re = 3900 is first performed. The Reynolds number was chosen in such a way that results can be compared with well-known experimental and simulation data. Flow over a cylinder at Re = 3900 has been extensively studied in literature. Lysenko et al. [18] reviewed the literature at the time for both LES and experimental work at Re = 3900. The experimental work of Lourenco and Shih [38] and Parnaudeau et al. [39] are the most widely used data to compare flow characteristics in the near-field wake behind the cylinder, while the Ong and Wallace [40] experiment is used for far-field comparison with simulation data. It has been observed that the span wise length of the computational domain can have a significant effect on simulation results at such Reynolds numbers. Kravchenko and Moin [41] studied the effect of span wise domain length and showed that the drag coefficient (C_D) predicted can vary 1.65 for a 2D simulation to 1.07 for a domain length of πD as shown in

www.manaraa.com

Recent DNS studies by Wissink and Rodi [42] show that increasing the spanwise size of the computational domain from 4D to 8D only marginally affect the profiles of turbulence statistics in the wake of the cylinder.

Table 2. The effect of grid points in span-wise direction (Nz) and span-wise length (Lz) on simulated Strouhal number (St) and average drag coefficient (CD) using LES (Kravchenko and Moin [41])

Case	N_z	L_z	$\overline{C}_D$	St
1	1	0	1.65	0.230
2	4	$\pi D/2$	1.36	0.190
4	8	πD	1.38	0.193
3	24	$\pi D/2$	1.07	0.212
5	48	πD	1.04	0.210
6[a]	48	πD	1.07	0.206
Expt	···	···	0.99±0.05 (1)	0.215±0.005 (2), (3) 0.21±0.005 (4)

[a]Coarse grid in radial and circumferential directions.

www.manaraa.com

3.2.1 Computational Model

The classical O-type grid is employed here, and is shown in Figure 31. The mesh design is mimicked from that used by Lysenko et al. [18]. The computational domain has a radius of 50*D*. The domain has a span-wise extension of πD, as was also used by Lysenko et al. [18]. The domain had slightly less than 3 million computational cells with 300×300 orthogonal grids in the cross-sectional plane and 24 cells in the span-wise direction. Grid points were clustered near the surface of the cylinder ($\Delta r/D \approx 10^{-3}$) with a grid expansion factor of 1.025 in the radial direction. The diameter of the cylinder (D) was chosen to be 1 m. The incoming flow velocity (U_∞) of air was 0.0589 m/s. Cyclic boundary condition were used for the front and back faces in the span-wise direction.

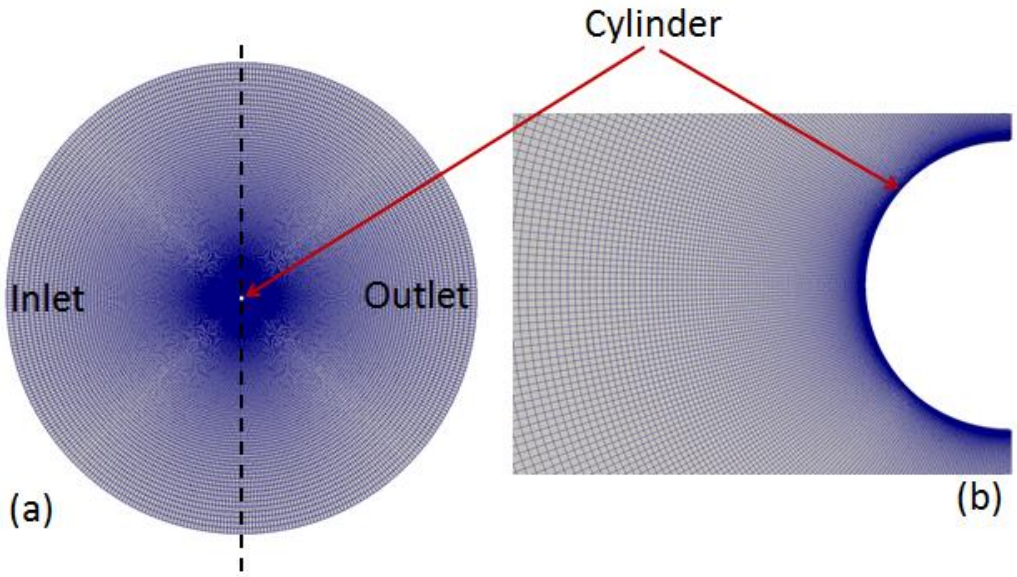

Figure 31. (a) The computational domain; and (b) Mesh near the surface of the cylinder

www.manaraa.com

The Sub-Grid Scale (SGS) model selected for the LES simulation was the Dynamic Local-averaged Smagorinsky model based on the experience of model selection studies conducted in the previous chapter. The LES simulation results was compared with the experimental measurements of Lourenco and Shih [38] and Parnaudeau et al. [39] for flow characteristics in the near-field wake behind the cylinder while for the far-field comparison the measurements of Ong and Wallace [40] was used. The simulation was run for about 300 vortex shedding cycles. Time-averaging of the flow statistics was started after approximately 15 vortex shedding cycles.

3.2.2 Results and Discussion

Figure 32 shows the distribution of vorticity magnitude at different time instances during a single vortex shedding cycle. Based on the Strouhal number (St) observed in the experiments and cylinder dimension in the simulation setup, the time period of one shedding cycle (t_c) was about 80s. Table 3 shows the minimum and maximum y^+ near the cylinder wall during a single vortex shedding cycle. The maximum y^+ value never exceeds 0.32. Thus the grid resolution in the viscous sublayer was adequate, and hence no wall modeling was required.

www.manaraa.com

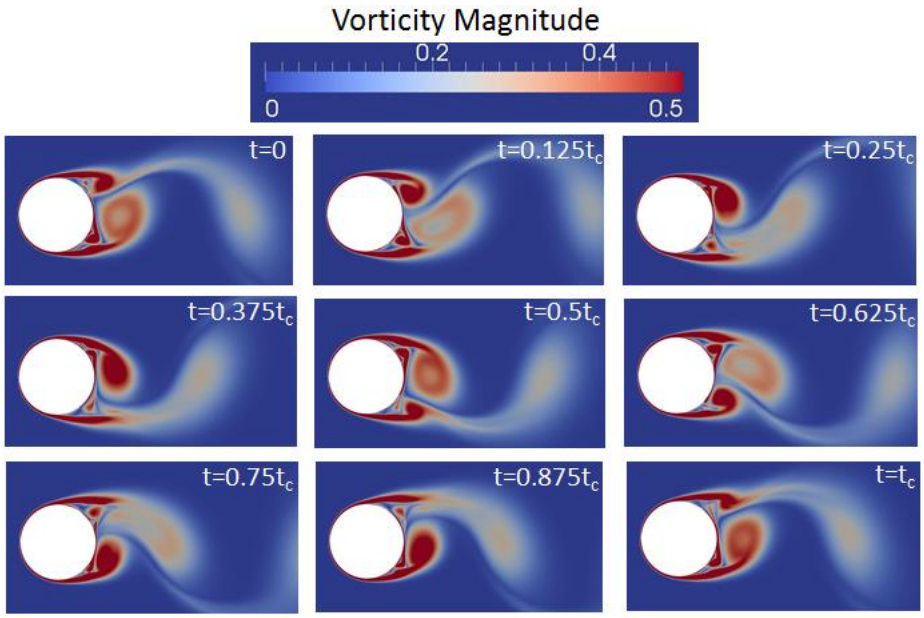

Figure 32. Contours of vorticity magnitude at different time instances during a single vortex shedding cycle

Table 3. The minimum and maximum y+ near the cylinder wall during a single vortex shedding

Time	Minimum	Maximum
0	0.0083	0.3052
0.125 tc	0.0103	0.3068
0.25 tc	0.0141	0.3177
0.375 tc	0.0105	0.3187
0.5 tc	0.0084	0.3092
0.625 tc	0.0092	0.3026
0.75 tc	0.0140	0.3154
0.875 tc	0.0078	0.3193
tc	0.0102	0.3124

www.manaraa.com

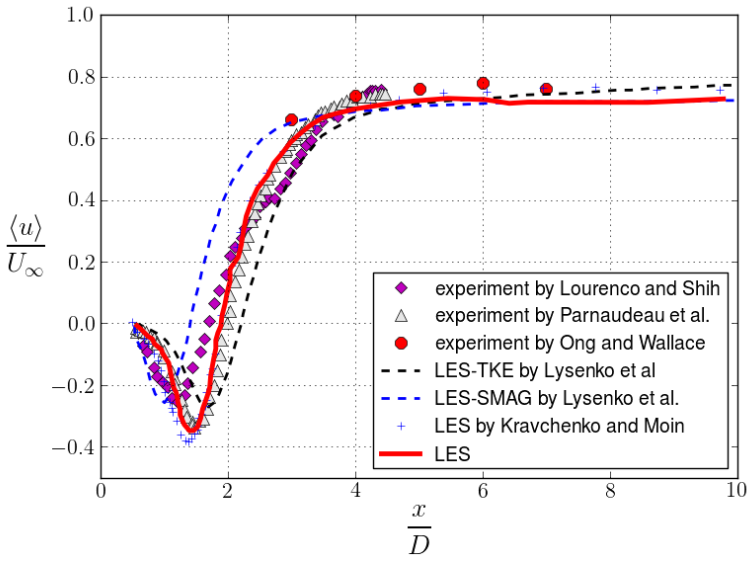

Figure 33. Comparison of mean stream-wise velocity in the wake centerline for isothermsalflow over a circular cylinder at Re = 3900. *x* =*D*/2 is the surface of the cylinder.

Figure 33 shows a comparison of stream-wise velocity in the wake centerline simulated for our case with published data from LES simulations and experimental measurements. The LES simulation of Lysenko et al. [18] with conventional Smagorinsky SGS model (LES-SMAG) and dynamic k-equation eddy viscosity subgrid scale model (LES-TKE) is shown in the figure along with the LES simulation of Kravchenko and Moin [41] simulation with a dynamic subgrid scale model. Lysenko et al. [18] obtained averaged turbulence statistics over 150 shedding cycles while Kravchenko and Moin [41] which is the closest to the data obtained statistics over approximately 7 vortex shedding cycles. Franke and Frank [43] concluded that more than 40 vortex shedding periods are required to obtain converged mean flow statistics. The experiments of Parnaudeau et al. [39] collected data of about 60 vortex shedding cycles to obtain averaged turbulence statistics.

www.manaraa.com

Lysenko et al. [18] and Lourenco and Shih [38] conducted measurements over 29 vortex shedding cycles. As pointed out by Lysenko et al. [18], the PIV data of Parnaudeau et al. [39] differed from those measured by Lourenco and Shih [38], but were consistent with HWA (Hot-Wire Anemometry) data of Ong and Wallace [40]. The LES-SMAG simulation of Lysenko et al. [18] would be the most appropriate LES simulation to compare with as time-averaged data over 150 vortex shedding cycles was presented. Our simulation results of mean stream-wise velocity compare well with the LES simulations of Lysenko et al. [18] with dynamic SGS model and the experiments of Parnaudeau et al. [39] Our LES simulation only used 24 cells in the span-wise direction compared to 64 cells by Lysenko et al. [18].

www.manaraa.com

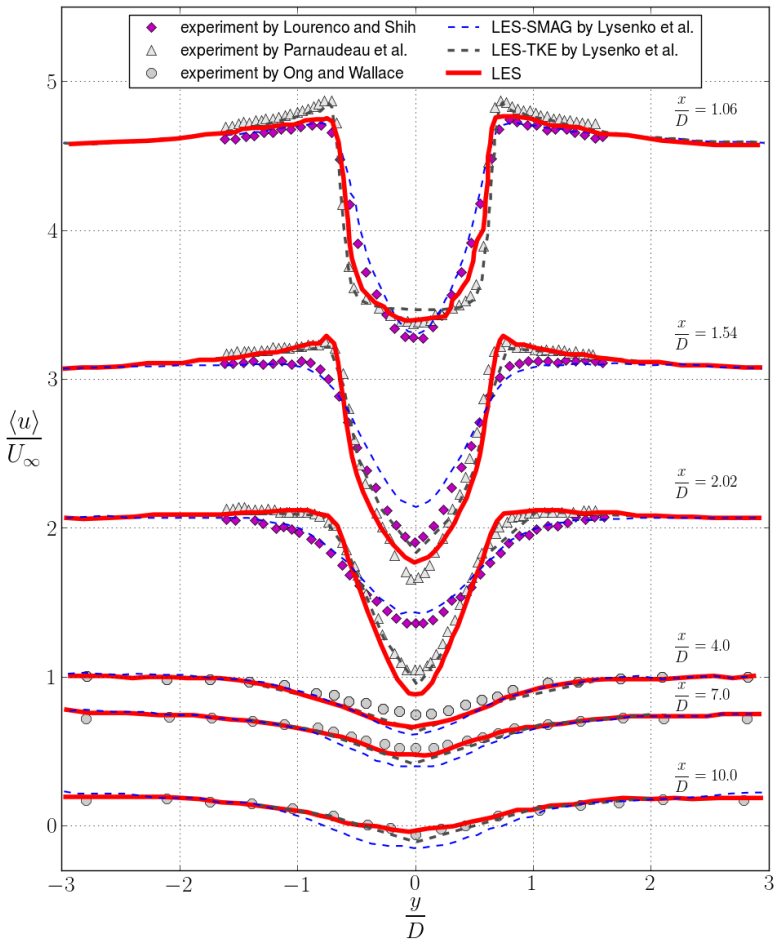

Figure 34. Comparison of mean stream-wise velocity at different locations in the wake of a circular cylinder at Re = 3900

Figure 33 and Figure 34 show the mean stream-wise and transverse velocities respectively. The figures compare the statistics in between $1 \leq x/D \leq 10$ with the experiments of Lourenco and Shih [38] and Parnaudeau et al. at three different downstream locations in the very near wake (x/D = 1.06, 1.54, 2.02) and with the experiments of Ong and Wallace at downstream locations of x/D = 4.0, 7.0, 10.0. The stream-wise velocity compared well with the measurements of Parnaudeau et

www.manaraa.com

al. and Ong and Wallace as well as LES simulation of Lysenko et al. with the dynamic SGS model. It is evident from the results of Lysenko et al. that the conventional Smagorinsky SGS model is not appropriate for simulating the flows over cylinder. Kravchenko and Moin also stated that simulations with dynamic SGS model agree better with experimental data compared to the conventional Smagorinsky model. Some discrepancies are observed for transverse velocities at x/D of 1.06 between our simulation and the simulations of Lysenko et al. with dynamic SGS model, which agreed well with the measurements of Parnaudeau et al. This is probably due to the use of only 24 cells in the span-wise direction for our simulation compared to 64 cells by Lysenko et al. Kravchenko and Moin observed that number of cells in the span-wise direction can significantly influence the turbulence statistics close to the cylinder and its effect is seen to be less significant at locations further downstream.

www.manaraa.com

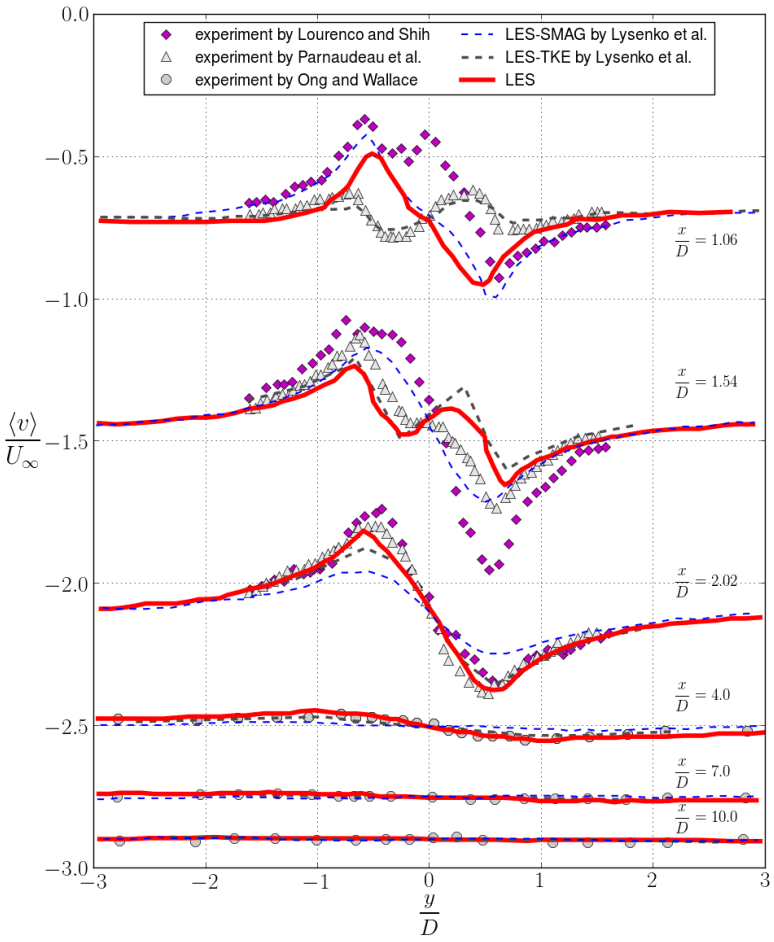

Figure 35. Mean transverse velocity at different locations in the wake of a circular cylinder at Re = 3900

The mean stream-wise and transverse velocity fluctuation at different downstream locations is shown in Figure 36 and Figure 37 respectively. As was seen for transverse velocity, the simulation results did not compare well with that measured by Parnaudeau et al. at x/D of 1.06 and 1.58, i.e. for locations very close to the cylinder. Even with 64 cells in the span-wise direction, Lysenko et al.'s simulation also showed similar comparison. The simulations generally under-

www.manaraa.com

predicted both the stream-wise and transverse velocity fluctuations at x/D locations of 1.06 and 1.58. However, for x/D location of 2.02, 4.0, 7.0 and 10.0, the LES simulations compared well with experimental data. The Strouhal number (St) and average drag coefficient (C_D) for our simulation 0.193 and 1.38 respectively, and matched exactly with published results of Kravchenko and Moin (refer to Table 1) with 24 cells in the span-wise direction.

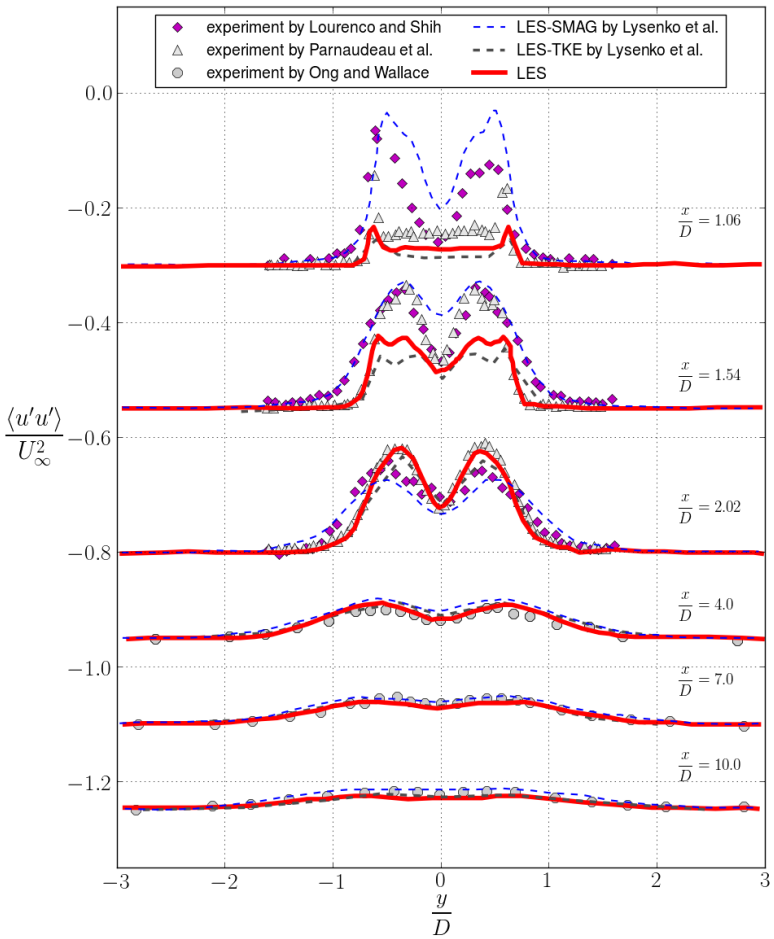

Figure 36. Stream-wise velocity fluctuations at different locations in the wake of a circular cylinder at Re = 3900

www.manaraa.com

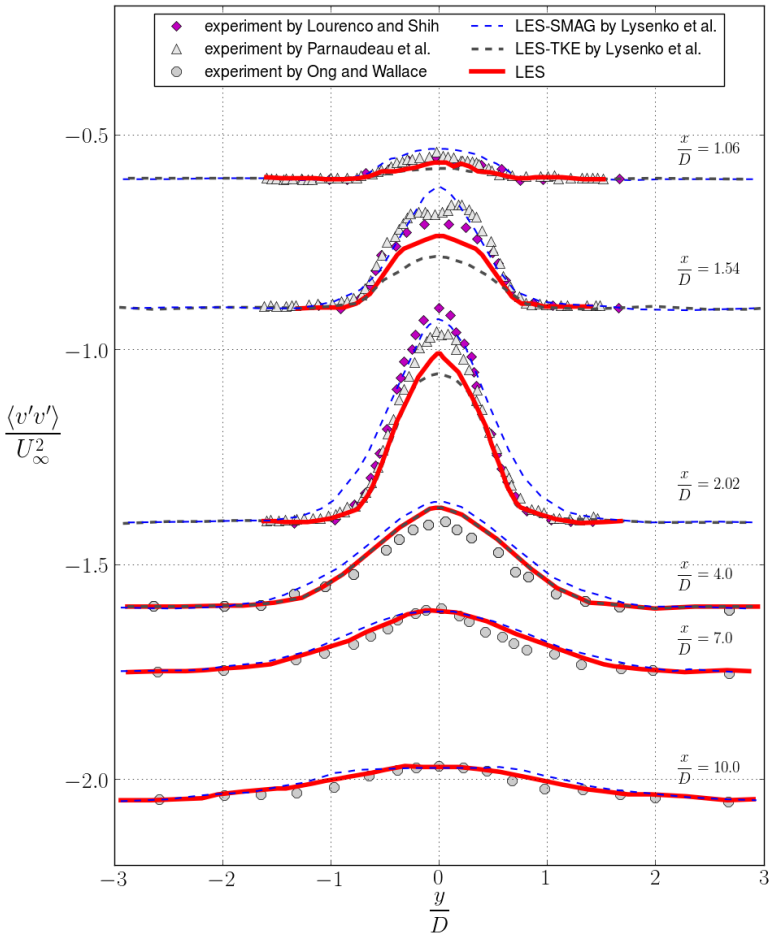

Figure 37. Transverse velocity fluctuations at different locations in the wake of a circular cylinder at Re = 3900

3.2.3 Remarks on Isothermal Cylinder Study

In general, CFD results from the open source computational fluid dynamics package, OpenFOAM, compared well with well-known sets of experimental data and LES simulations for

www.manaraa.com

isothermal flow over a cylinder for Re = 3900. Also, isothermal LES jet simulation in the previous chapter compared remarkably well with benchmark experiment of HCG [14]. Since isothermal simulations compared extremely well with published work, our next efforts would focus on exploring and analyzing flow past a non-isothermal cylinder in detail, in accordance with the targets and framework of the current research project.

3.3 LES SIMULATION OF NON-ISOTHERMAL FLOW PAST A CYLINDER

3.3.1 Computational Model

Exact similar classical O-type grid, as shown in Figure 31 as used by Lysenko et al.[18], is employed for the simulation. The computational domain has a radius of 50 D. The domain has a span-wise extension of π D as was used by Lysenko et al.[18]. The domain has slightly less than 3M computational cells with 24 cells in the span-wise direction. Grid points are clustered near the surface of the cylinder ($\Delta r/D \approx 10^{-3}$) with a grid expansion factor of 1.025 in the radial direction. Cyclic boundary conditions are used for the front and back faces in the span-wise direction. A non-reflective boundary condition is employed for the outlet condition to prevent numerical waves coming inside of the computational domain. Similar to the experimental set up, a constant wall temperature is used for the boundary condition. The temperature difference between the heated surface and incoming flow is fixed to 25°C.

www.manaraa.com

The Sub-Grid Scale (SGS) model selected for the LES simulation is the Dynamic Local-averaged Smagorinsky model based on the experience of model selection studies conducted in the last chapter. Compressible sets of Navier–Stokes equations are solved by OpenFOAM. Specifically, the PIMPLE version of PISO (Pressure Implicit with Splitting of Operators) algorithm is employed as an efficient method to solve the Navier-Stokes equations in unsteady problems. The PISO algorithm is a pressure-velocity calculation method. The simulation is run for about 300 vortex shedding cycles. Time-averaging of the flow statistics is started after approximately 15 vortex shedding cycles. Turbulence intensity of the incoming flow has also been matched to that reported from the experiment of [34], namely 0.5%.

3.3.2 Results and Discussion

Figure 38 portrays instantaneous vorticity magnitude contours in the near-wake of the cylinder at the three Reynolds numbers. Even though the difference between Reynolds numbers is not very large, yet the structural change in the cylinder wake as the Reynolds number increases is visible with comparison of these contours. It can be seen that, as the Reynolds number increases, the location at which the separated shear layer becomes destabilized moves upstream. This is particularly noticeable when comparing the result for Re = 7400 with those from the two lower Reynolds numbers. Large-scale vortex-shedding is observed at all three Reynolds numbers.

www.manaraa.com

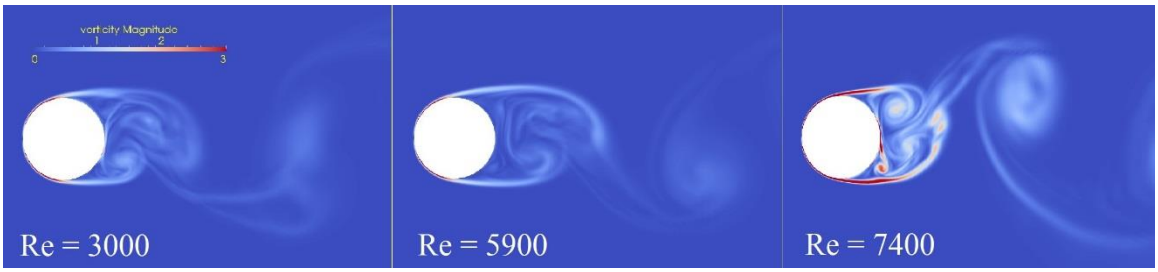

Figure 38. Contours of instantaneous vorticity magnitude in the near-wake for different Reynolds numbers

Instantaneous temperature fields are portrayed in Figure 39 in the near-wake region of the cylinder. This contour plots and Figure 38 well portray that the instability leads to stronger turbulent mixing of momentum in the near-wake, which causes drop of the size of the mean recirculation region. As we can see shear layer becomes unstable and mixing of momentum leads to the mixing of the scalar quantity (temperature) and as previously discussed, it causes heat transfer enhancement.

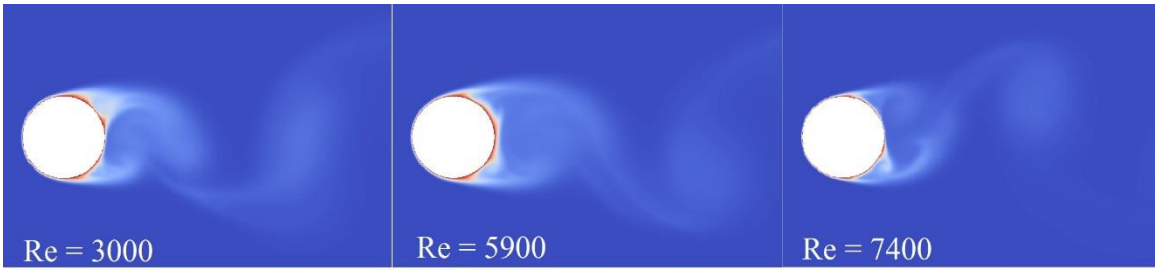

Figure 39. Contours of instantaneous temperature in the near-wake for different Reynolds numbers

The distribution of the time-averaged Nusselt number and its r.m.s. value are key metrics to compare with experimental data. Figure 40 shows the results of this comparison and reveal

www.manaraa.com

excellent agreement for both quantities. The LES data accurately captures the laminar flow region for φ < 80°, where φ is the angle from the stagnation point of the cylinder. The average Nusselt number is highest at the stagnation point (φ = 0°) where the thermal boundary layer is thinnest, and then shows a decreasing trend until φ is between 90 and 100°. The magnitude of the Nusselt number fluctuations up to this point is very small, both experimentally and as suggested by the LES data, further highlighting the fact that this region of flow can be classified as laminar. The increase in both average and fluctuating Nusselt numbers coincides with the flow fluctuations resulting from the separated shear. The magnitude of heat transfer increases and reaches a second peak at the rear stagnation point (φ = 180°). Although the average Nusselt number at the stagnation point is fairly independent of Reynolds number ($\overline{Nu}/Re^{0.5} \approx 1$ at φ = 0° for all three cases), this is clearly not case when considering behavior at the rear stagnation point. For comparison, the average Nusselt number at φ = 180° is approximately 0.2, 0.4, and 0.6 for Re = 3000, 5900, and 7400, respectively. Similarly, for the fluctuating Nusselt number, the stagnation point value is roughly the same for all three Reynolds numbers, and the rear value increases with Re. It is interesting to note that the value at φ = 180° is roughly 60-65% of the time average Nusselt number. In other words, the Reynolds number dependence is the same for both the fluctuating and average Nusselt number trends. For a Re = 7400, the sharp upswing in heat transfer is not continuously monotonic. In other words, there is an intermediate peak reached around φ = 115°, after which a local minimum is reach quickly, followed by a subsequent increase in both the fluctuating and time averaged Nusselt number graphs. This indicates that an additional reattachment point near the rear of the cylinder is first observed at Reynolds number around 7400. A fluctuating pressure

www.manaraa.com

distribution around a circular cylinder is known to have a local maximum at $\varphi = 105°$, at which point the reattached reverse flow separates. This maximum disappears below Re = 6000-8000, corresponding to the range for which the reattached flow disappears [34, 44]. Therefore, the LES model is capturing the important physics, not only of the flow, but for the expected thermal behavior as well.

www.manaraa.com

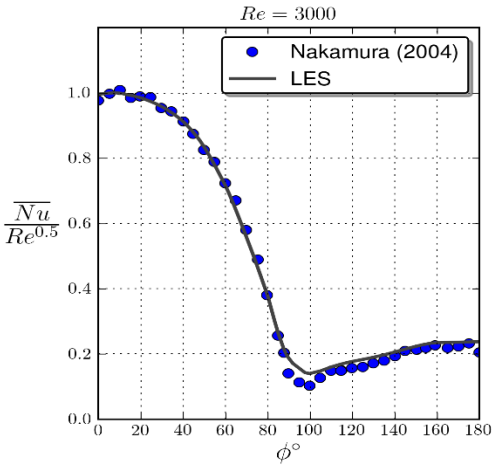

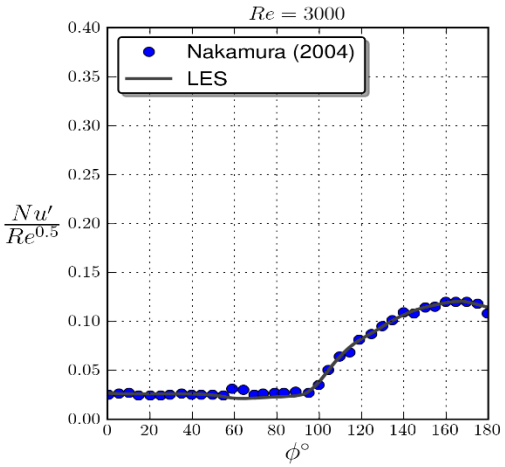

www.manaraa.com

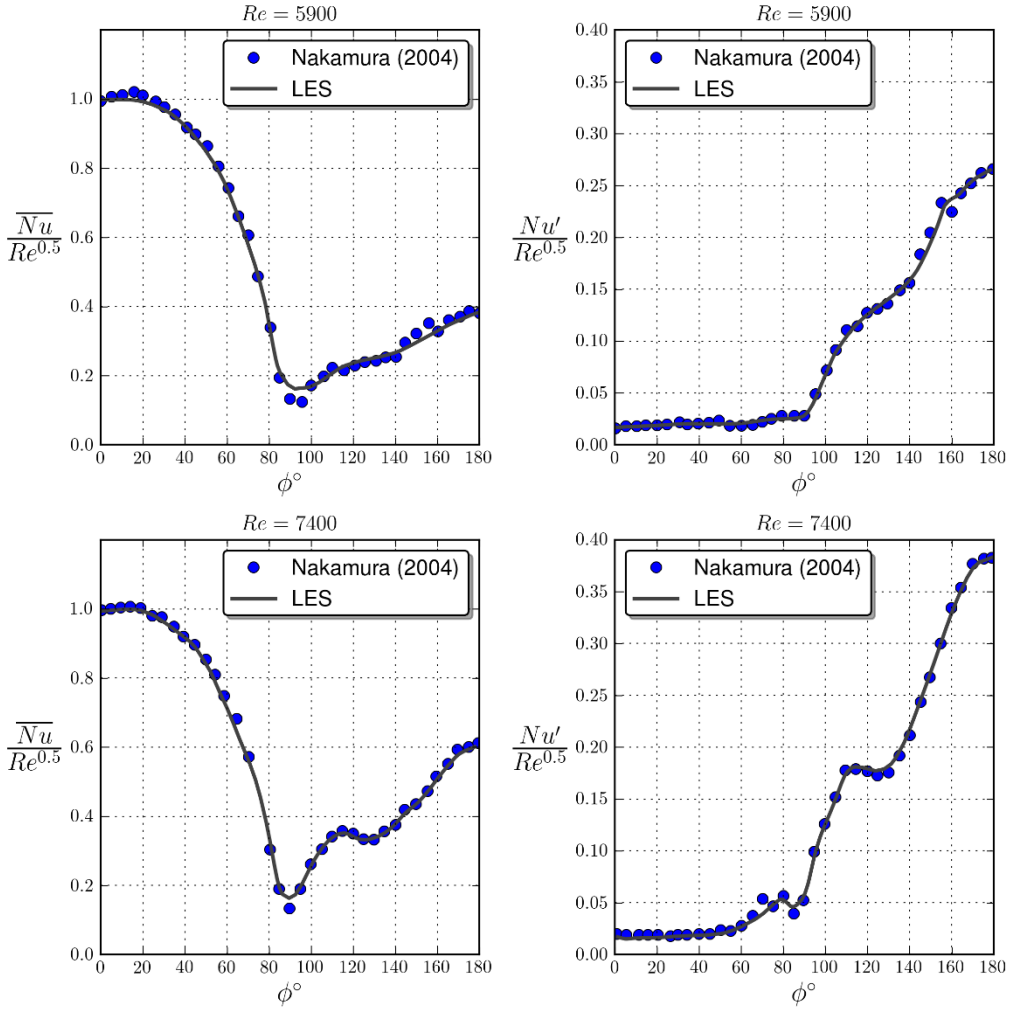

Figure 40. Time-averaged and r.m.s Nusselt number distributions around a circular cylinder for Reynolds number of 3000, 5900 and 7400.

Figure 41 shows time traces of the fluctuating Nusselt number at Reynolds number of 5900 where Nakamura and Iragashi [34] reported similar data at the same Reynolds number. The data is collected at several azimuthal location at the mid-span of cylinder. As can be seen at $\varphi = 70°$ the point is in the laminar region since fluctuations are small enough to be neglected. As φ is increased,

www.manaraa.com

both the flow features and heat transfer is affected by the instability of separated shear layer and vortex shedding. As boundary layer instability grows 150° < φ < 180° the fluctuating Nusselt number become much larger. The same observation is made by Nakamura and Iragashi [34].

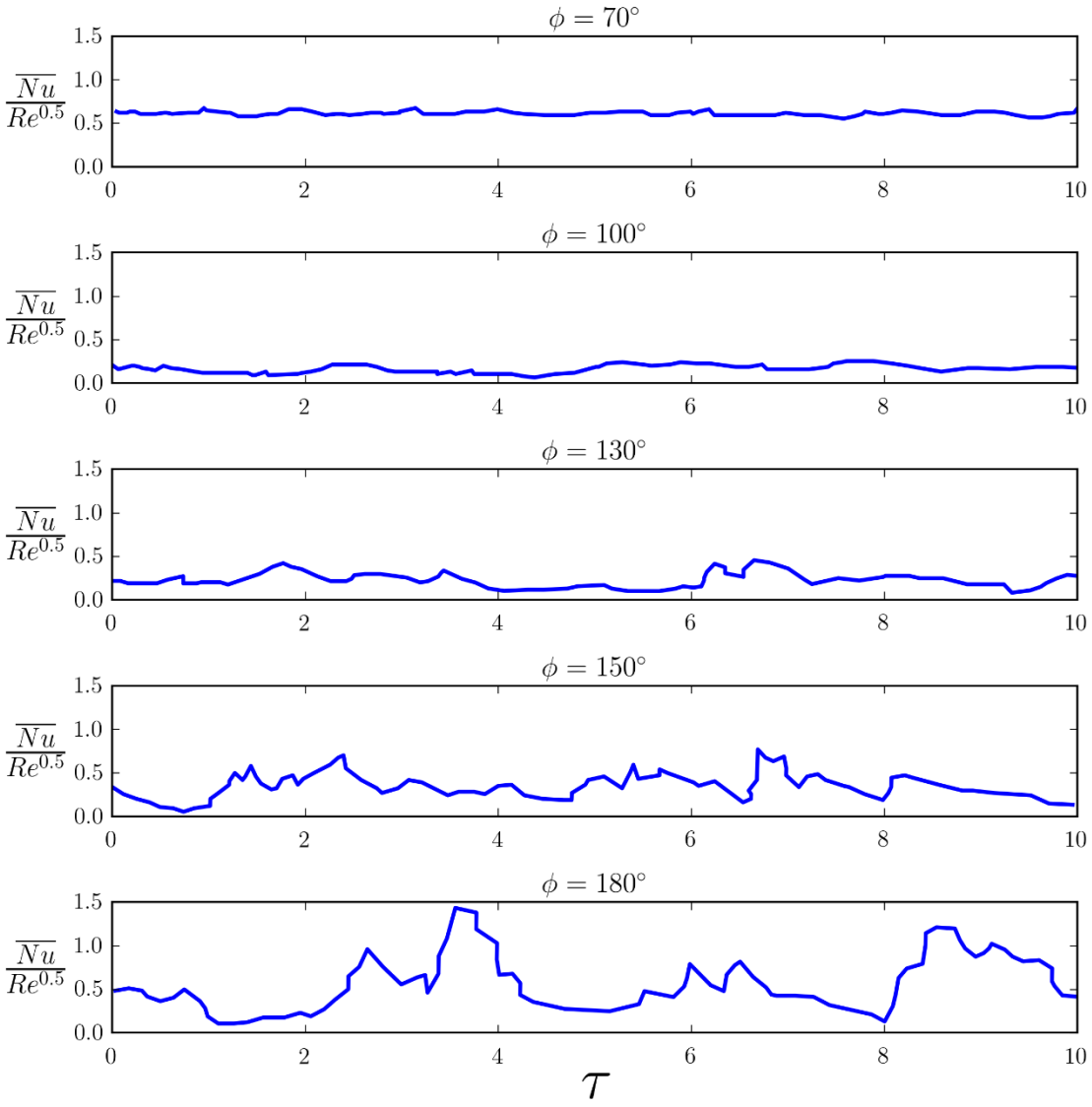

Figure 41. Time-histories of the instantaneous r.m.s Nusselt number for Re=5900.

www.manaraa.com

3.4 CONCLUSIONS

The LES of turbulent flow and heat transfer around a circular cylinder was conducted using OpenFoam at three Reynolds numbers (Re = 3000, 5900, 7400). From these results, it can be seen that the physics of the heat transfer are captured very faithfully. The heat transfer characteristics of the laminar boundary layer upstream of the separation point as well as the entire region behind cylinder is accurately modeled. Excellent agreement is seen with the experimental data regarding time-averaged and r.m.s. Nusselt numbers. The sharp increase both in the mean Nusselt number and the r.m.s. fluctuating Nusselt number is also reproduced with high fidelity. Strong correlation between the heat transfer characteristics and the underlying flow characteristics is also confirmed.

Future and more detailed LES related studies should also be conducted. In particular, other LES studies should be done with higher Reynolds numbers and quantifying the metrics of importance as a function of upstream turbulence intensity. Also, the effect of the span-wise cell divisions should be considered. These additional studies will serve as better understanding of both fundamentally and practically important problems.

www.manaraa.com

4.0 LES OF NON-ISOTHERMAL TURBULENT ROUND JET

The final goal of this thesis is to study a non-isothermal turbulent jet. In order to achieve this, a non-isothermal round free jet at Reynolds number of 16,000 is computed by Large Eddy Simulation (LES). The mean temperature at the jet nozzle is approximately 50K above ambient. The enclosure within which the jet is confined has been selected large enough so that the results can be compared with well-known experimental studies available in the literature. The Sub-Grid Scale (SGS) model chosen within the LES framework is a variant of the dynamic Smagorinsky model for a compressible simulation. The effect of inlet flow profile and turbulent fluctuations on the evolution of the jet have been analyzed in detail by performing a separate large eddy simulation of the flow in the nozzle upstream of the jet inlet to accurately determine the inlet turbulent spectra. Properly specifying the turbulent fluctuations at the jet inlet was found to play a vital role in accurately predicting key metrics throughout the computational domain. The LES results of this study include first and higher order statistics of velocities and temperature.

4.1 INTRODUCTION

Non-isothermal round turbulent jets are widely used in a number of various applications including ventilation, drying, combustion, cooling, propulsion, etc. The mixing between jet and ambient fluid is of primary importance where efficient mixing of mass, momentum and heat are

www.manaraa.com

easy to generate. Although in general, turbulent free jets have been a canonical flow from a scientific standpoint for many decades, a firm knowledge of non-isothermal jets is required for many useful technological applications

Similar to isothermal turbulent jets, experimental investigation of non-isothermal turbulent jets also has a rich history. One of the first comprehensive studies was conducted by Corrsin & Kistler [45], and years later in more details, followed by another key investigation by Chevray and Tutu [46]. In both of these studies, the authors made detailed investigation of temperature and velocity fields in a round heated air jet issuing from a contraction into an insulated test section. Values of the mean velocity and temperature (above ambient) at the jet exit were 25 m/s and 20°C respectively, while measured turbulence intensity at the same location was around 0.5%. Those two mentioned articles had been among the very few measurements aimed at quantifying the Reynolds shear stress and heat flux in a turbulent round jet. Chua and Antonia [47] measured those quantities as well as the turbulent Prandtl number for a circular jet at a Reynolds number of 17,700. Antonia and Mi [48] also made some measurements of temperature dissipation with the aid of a parallel cold wire for a jet at Reynolds number of 1.4×10^4. They measured the temperature derivative and dissipation in each of the three directions and found that the radial and azimuthal values of temperature dissipations were almost equal and only slightly larger than the axial component. The subsequent departure from isotropy of the temperature dissipation was found to be very minor. The influence of initial flow conditions on the passive scalar field of a slightly heated turbulent free jet was investigated by Mi et al. [49]. Detailed experimental data was reported for jets at a Reynolds number of 16,000 issuing from two nozzle types: a smooth contraction and

www.manaraa.com

a long straight pipe. Significant differences between the flows issuing from the two nozzles were found across the flow region covering an axial range from 0 to 70 jet exit diameters downstream. Mi and Nathan[50] complimented this study by investigating the centerline evolutions of turbulent statistical properties of non-isothermal air jets issuing from nine differently-shaped nozzles. The loss of jet axisymmetry at the jet exit caused faster mean velocity decay, and enhanced the growth of the fluctuating intensity in the near-field. However, the asymptotic decay rate of the centerline velocity in the far-field seemed to remain independent of nozzle shape.

In spite of various experimental investigations, the number of computational simulations is surprisingly limited. Among those rare simulations, Smith et al. [51] did a RANS simulation to evaluate capability of the k-ε turbulence model to predict flow physics influenced by variation of nozzle shape in heated turbulent round jets. Not surprisingly, it was found that RANS is incapable of correctly predicting key aspects of the near-field flow in addition to the rates of spread and decay caused by changes to nozzle shape. Suto et al. [52] performed LES of four different Reynolds numbers ranging from 1200 to 10^6 for a heated jet. Dynamic Smagorinsky model was found to be in better agreement of the mean velocity than the standard Smagorinsky model. However, discrepancies were observed between LES and experimental measurements of scalar fluctuations intensity in the near-field. Colombo et al. [53] used LES implemented in FLUENT code to simulate a non-isothermal air jet at Reynolds number of 95500. Mean velocity, mean temperature and second order moments of velocity components calculated from LES were compared with different available experimental results. Key features of the non-isothermal jets like temperature fluctuations and its r.m.s. are absent in their studies.

www.manaraa.com

The main goal of the current chapter is to verify computationally the experimental data of Mi et al. [49] for a non-isothermal axisymmetric jet flow and to resolve the ambiguity regarding the differences between these results and other experimental regarding the presence of a hump in centerline r.m.s of the temperature fluctuations over mean temperature in near-filed. And also, to verify if a comprehensive LES work is attainable to capture the physics of both far-filed and near-filed of a non-isothermal jets. To address the above objectives two separate LES studies are conducted one for precursor of the jet to provide correct inlet condition for the second and one LES study corresponding to Mi et al. [49] experimental measurements..

4.2 COMPUTATIONAL MODEL

Large eddy simulation is conducted for better understanding of a non-isothermal turbulent jet and compared against the measured data of Mi et al.[49]. In order to mimic the experimental work, the non-isothermal round jet diameter is set to D = 14 mm and is 50 K above the ambient temperature of 288 K. Similar to the isothermal studies of Chapter two, the LES domain here is 100 D in length from the jet nozzle to the outlet of the domain. This enables direct comparison with data from Mi et al.[49], who made measurements up to 70 D downstream of the jet nozzle. The overall diameter of the domain is 55 D. The Reynolds number (Re_D) of the jet based on the average jet velocity and diameter at the exit of contraction nozzle is 16,000. The back and side wall temperatures of the simulation domain are set to ambient temperatures (288 K). Accurate

www.manaraa.com

fluctuating inflow velocity conditions are used from the precursor contraction nozzle simulation which similar to that of mentioned in the previous quarter. Adjustable time stepping with maximum courant number of 0.4 is used for the simulations. The compressible non-isothermal round jet simulation is performed using the rhoPimpleFoam compressible solver in OpenFOAM. The 'dynLocalAverageSmagorinsky' SGS (Sub-Grid Scale) model is used for LES. The incompressible 'dynLocalAverageSmagorinsky' SGS model gave accurate predictions of turbulent statistics for both an isothermal round jet as well as non-isothermal flow past a cylinder as reported in the previous chapters, and for this reason, OpenFOAM was modified to accommodate this model here as well.

A RANS simulation is first performed in order to initialize the flow field and temperatures inside the domain. This approach also motivates the mesh creation process for LES through adjusting the local mesh size depending on the turbulence length scale found from RANS data.

The mesh used for the simulation is similar to that of used for isothermal jet. The domain has just over 16 million cells. As seen in Figure 42, different mesh size is applied in the axial direction from the inlet to the location $x = 15\ D$ downstream to ensure that the inner core of the jet is well resolved at entry. For the remainder of the downstream domain ($15\ D < x < 100\ D$), the axial mesh size is $D/8$. Using a compressible solver enables the use of non-reflecting boundary condition at the outlet. In the radial direction, a 15 × 15 uniform square grid is used at the center of the jet inlet in a manner similar to the isothermal jet mesh design. Each square cell in this Cartesian grid has side length equal to $D/25\sqrt{2}$ size. The very center cell of this grid is collocated with the overall domain centerline, thereby eliminating the need to interpolate for any centerline

www.manaraa.com

data for which experimental results are widely available. As can be seen in Figure 42 three additional radial layers of cells exist between the bounds of the Cartesian grid and the edge of the circular inlet ($r = D/2$). Outside of this circular inlet, a uniform mesh size is used between $r = D/2$ and $r = D$. The mesh size in this region is similar to the average mesh size contained within the jet diameter. An expanding grid is then used from $r = D$ to $r = 5\,D$. A uniform structured square grid size of $D/8$ was then applied from $r = 5D$ to the outside edge of the computational domain ($r = 27.5\,D$). The number of azimuthal divisions is dictated by the 15 × 15 Cartesian array (4 × 15 = 60 divisions), which is found to be more than adequate for the isothermal work.

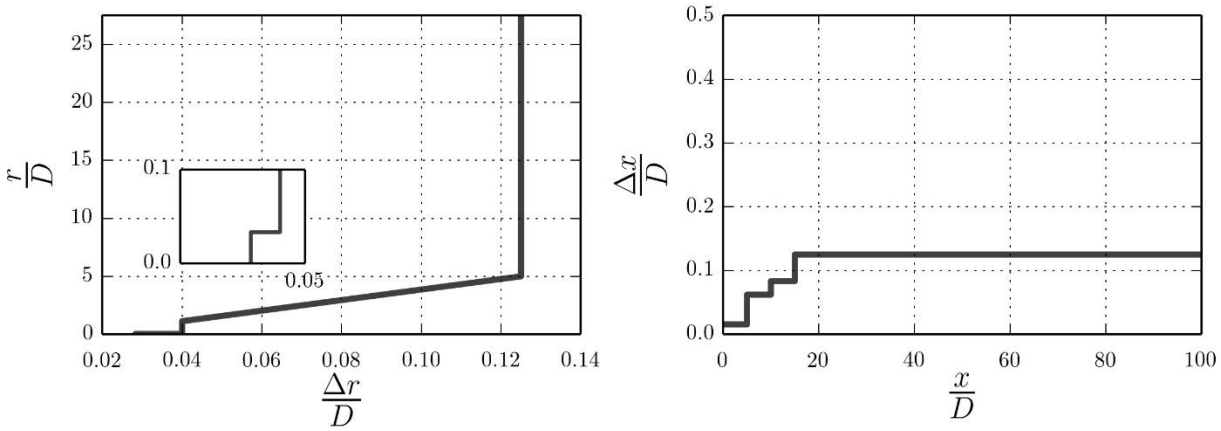

Figure 42. Mesh spacing in radial and axial direction. The grid is symmetric in respect to the jet axis

4.3 PRECURSOR SIMULATION OF NOZZLE FLOW

In their experiments, Mi et al. [49] used two different nozzles: a long straight pipe and a smooth contraction, the latter of which is the subject of current study. The contraction begins with

www.manaraa.com

a duct opening of 80 mm, which transitions down to the exit jet diameter of 14 mm. A faithful model for this contraction is created and shown in Figure 43. Tetrahedral cells were used to mesh the contraction geometry. The model had a total of 2.02 million cells. A very low value of turbulent intensity (with scale of 0.001) is prescribed at the inlet of the contraction model as would be expected close to the screen mesh of a wind tunnel [14]. Instead of modeling the large enclosure downstream of the nozzle, the flow is directed into a domain with a diameter 25 times the size of the jet diameter, in order to reduce computational costs. The flow inside the contraction domain is first initialized with steady state RANS data. Isothermal wall boundary conditions are used for entire contraction. The mesh near the wall is fine enough ($y^+ = 0.01$) to avoid any needs of a wall model. This mesh resolution is very computationally expensive, but it finds to be the only attainable solution for providing the correct inlet boundary condition for non-isothermal jets as DDES and other methods failed. In addition to velocities and temperature fluctuations, SGS measurements from contraction model shown to play vital role to precisely capture the near-field physics of the problem particularly r.m.s of temperature at centerline. rhoPimpleFoam solver with same SGS model is then used to obtain accurate flow conditions at the jet nozzle.

www.manaraa.com

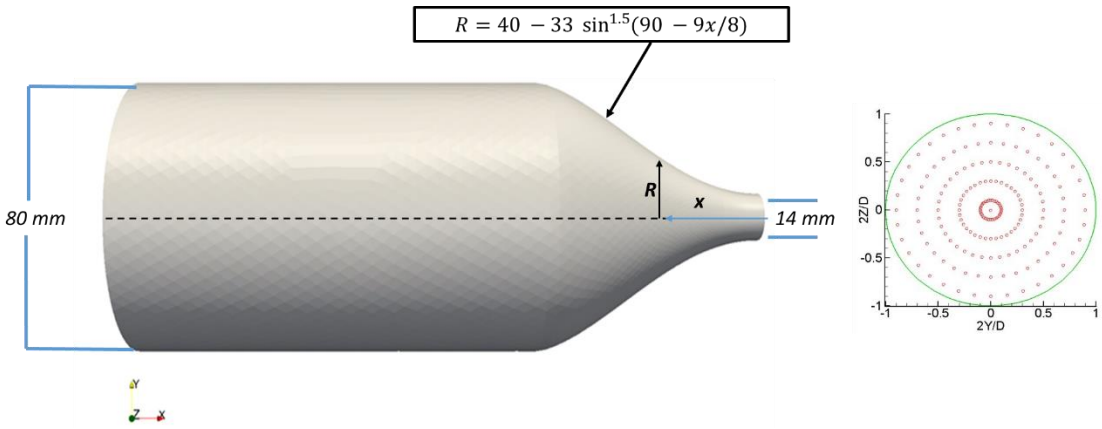

Figure 43. Computational model of the upstream contraction used in the experiments of Mi et al.[49]

Similar to what has been done in chapter 2, adjustable time stepping is used for the contraction simulation with maximum Courant number set at 0.4. As illustrated in Figure 43, transient velocity data is probed and saved at 181 locations (5 equally spaced radial locations at 10° angular increments at the nozzle exit plane as well as center of the jet to precisely capture and then feed inlet boundary condition of the jet). It should be noted that in all approaching figures "domain only" legend refers to inlet of the jet from DES which only provides velocity fluctuations, while "domain and contraction" legend talks about flow simulation with inlet condition consists of velocities, temperatures and SGS model calculated by separate LES model of contraction.

www.manaraa.com

4.4 RESULTS AND DISCUSSION

Figure 44 shows the axial variation of temperature normalized with respect to the mean inlet temperature of the jet. The variable θ is the difference between the temperature at a point and the ambient temperature. A good agreement between LES and experimental data can be seen particularly in downstream locations where the self-similar region is achieved which located after 20*D* downstream location of the domain. From this figure, the virtual organ (x_{01}) and decay constant (K_1) are determined as 3.58 d_e and 4.37 respectively which is in great agreement with the reported data of Mi et al. [49], calculated as 3.5 d_e and 4.48 respectively. Effective diameter d_e, is defined in Mi et al.[49]. The authors of that experimental paper argued that since the ratio of Gr/Re^2 (Gr = Grashof number) at the jet exit was extremely small for their experiment ($Gr/Re^2 \approx$ 10-5), the effect of buoyancy was negligible and thus the measured temperature field would be similar to that observed for a passive contaminant/tracer. Figure 44 also shows that our simulation data agrees well with the results of Mi et al. as we can expected, it means that the temperature calculation by LES is correctly assumed passive scalar. Also as seen in this figure, specifying accurate inlet condition from contraction model significantly improves the near-field data predictions.

Figure 45 depicts a different form of the normalized mean temperature and it shows that beyond downstream location of 10 *D*, the LES result is in a very good agreement with experimental measurements. Although the near-field data does not match perfectly, the behavior of both experimental and LES are extremely similar. Once more, the effect of including a contraction LES

www.manaraa.com

is noticeable, especially in near-field. This better prediction has an impact both in terms of the mean temperature as well as the virtual organ (x_{01}) values.

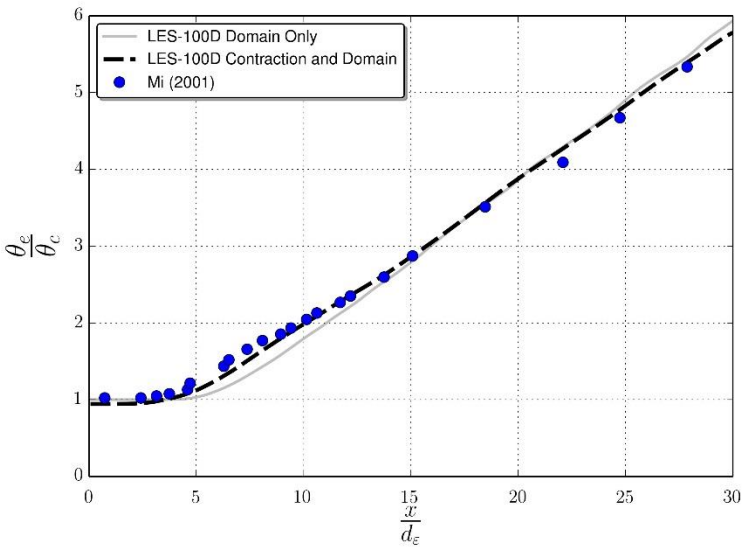

Figure 44. Centerline normalized inverse temperature

www.manaraa.com

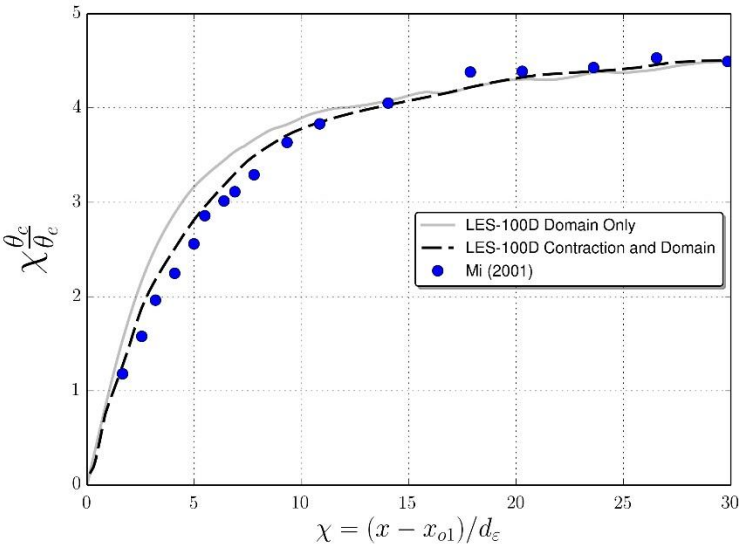

Figure 45. Streamwise versions of the normalized temperature mean

Figure 46 displays the spreading rate of the LES jet from the streamwise variations of the temperature half-radius $r_{1/2}$ at which is the location where the value of temperature is equal to half of the centerline temperature. The spreading rate of the half-radius is 0.115 which is very close to its experimental value of 0.11 reported by Mi et al.[49].

Figure 47 shows the radial variation of temperature for different axial locations of compressible LES simulation with temperature dependent fluid properties. The LES self-similar behavior of temperature have been captured well and also agrees well with data of Mi et al[49]. It seems that experimental results reach to ambient temperature sooner as go farther from centerline in compare with LES data. Further investigation and comparison with other experimental data should perform in future. The computational domain on the other hand seems to be large enough

www.manaraa.com

since self-similar behavior capture well and also LES results in radial direction agree well with experimental data.

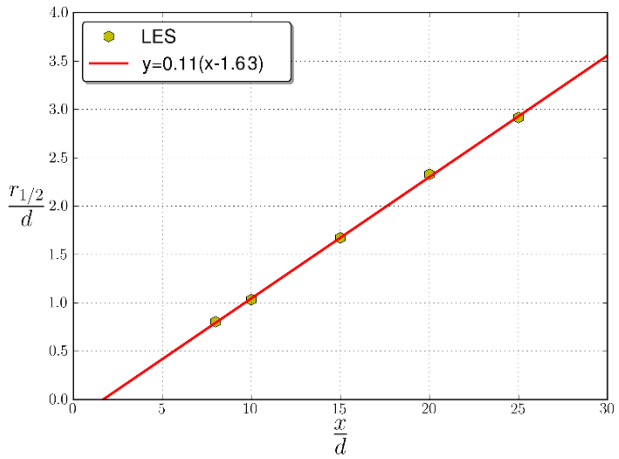

Figure 46. Streamwise versions of scalar half-radius

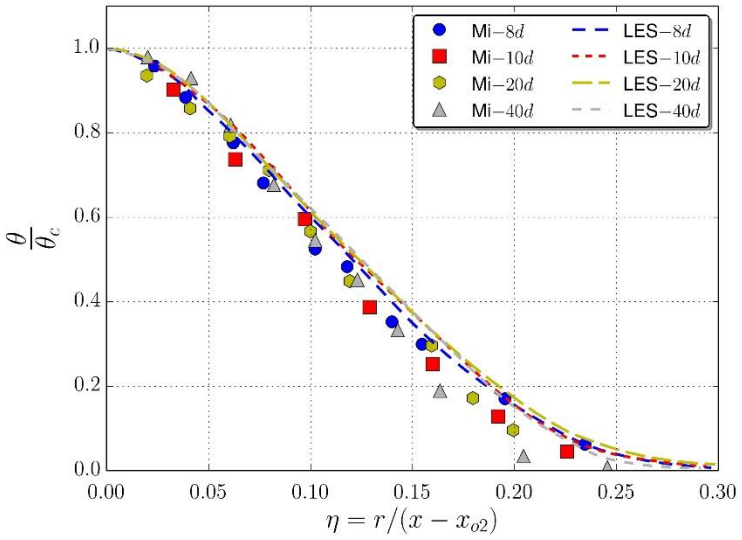

Figure 47. Radial profile of normalized mean temperature at several locations

www.manaraa.com

Figure 48 and Figure 49 compare the streamwise development of the centerline r.m.s. temperature fluctuations for the jet. Two normalization procedures are shown. The normalization by the exit mean temperature gives a reference for the absolute intensity of temperature fluctuations, while the locally normalized result provides a ratio which has been found by previous researchers to asymptote to a constant in the self-similar far-field region. As seen from Figure 48, the effect of contraction simulation on the precisely prediction of r.m.s temperature is vital. It is the main reason why all the previous computational studies (both RANS and LES) failed to accurately capture the physics of the problem.

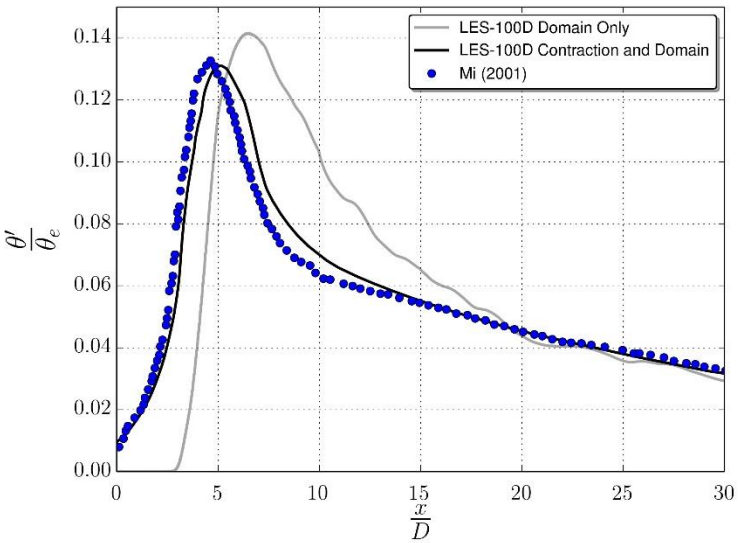

Figure 48. Streamwise variation of the temperature r.m.s. along the jet centerline

www.manaraa.com

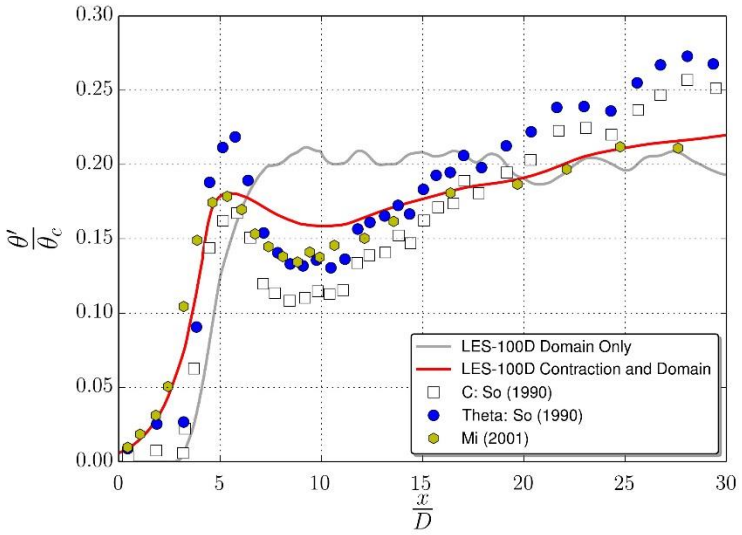

Figure 49. Streamwise variation of the temperature r.m.s. over centerline along the jet centerline

Figure 49 shows that for a jet coming from a smooth contraction nozzle, a local maximum, or a hump, is existing in the near-field. This observation also repeated in concentration data of So et al.[54]. On the other hand, there is no corresponding hump in a jet issuing from pipe as comprehensively mentioned in Mi et al.[49]. From Figure 49, it can be seen that presenting hump in both experimental and LES data is associated with the initial conditions which is in contrast with what some previous studies mentioned as experimental errors [55, 56]. Mi et al.[49] argued that for a jet issuing from a smooth contraction, strong large-scale “engulfment” of ambient `cold' air by the highly coherent vortex structures results in a high amplitude of the temperature fluctuations or the hump. By contrast, for jet coming from a pipe, the shortage of the large-scale coherent structures causes a fairly weak “engulfment” of surrounding `cold' air into the jet in near-field region.

www.manaraa.com

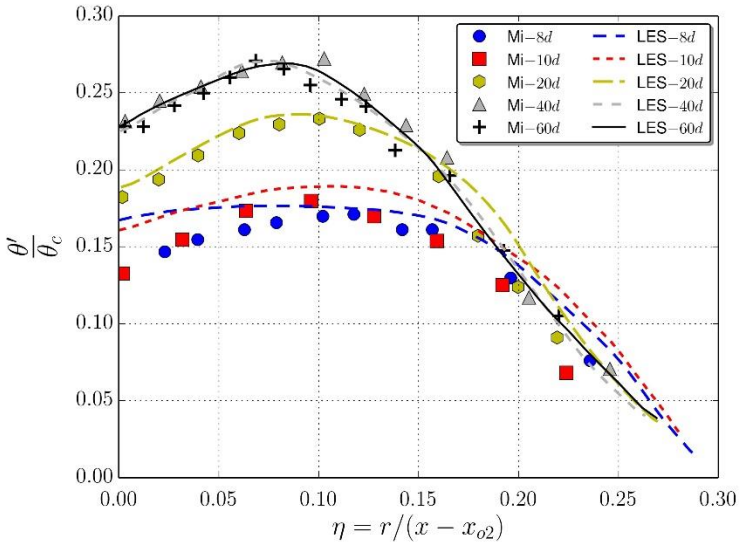

Figure 50. Radial profiles of the normalized temperature r.m.s. over centerline

Once again, the effect of contraction simulation is noticeable in Figure 49, accurately feeding the inlet condition results in near-field data improvement. This includes close to inlet data improvement as well as capturing the hump. The difference between Mi et al.[49] data and LES can be pointed to the fact that experimentally isothermal condition is impossible and also the effect of SGS seen to be very significant for LES improvement. Also, the main difference between DES and LES contraction simulation regarding the hump is coming from the better predication of inverse of temperature by LES as can be seen in Figure 44.

Figure 50 presents radial profiles of the normalized r.m.s. temperature fluctuations over centerline mean temperature. Relative to the mean temperature field, the r.m.s. temperature

www.manaraa.com

develops to the self-similar state further downstream from the nozzle exit. Similar to experimental data the self-similar state of the r.m.s. scalar is reached at $x > 40D$ for the LES case.

4.5 CONCLUSIONS

The present study has explored large eddy simulation of non-isothermal axisymmetric free jet similar to experimental study of Mi at el.[49]. The present LES is conducted at a Reynolds number of 16 000 using a compressible solver in OpenFOAM. The present study has revealed that to correctly simulate the turbulent scalar properties throughout the jet flow field in LES, very accurate inlet condition should be provided. Existing of the hump for jet issuing from the contraction is not only a noise but also for correctly capturing of that the separate contraction simulation have been conducted and data from this simulation feeds accurately as inlet condition for large domain simulation of main LES.

www.manaraa.com

5.0 CONTRIBUTIONS AND FUTURE WORK

The highly detailed LES studies in this thesis provide a critical first step in establishing validated models for turbulent mixing in nuclear applications. Specifically, the following contributions are made:

- In round turbulent jets, turbulence statistics, particularly third order moments and the energy budget, are shown to be influenced by Reynolds number.
- An intimate tie is established between the accuracy of the inlet conditions and that of the near-field structure prediction.
- The upstream flow modeling, even though computationally expensive in LES, provides key insights into the physics tied to an isothermal and non-isothermal turbulent round jet.
- In addition to temperature and velocity fluctuation as inlet condition, SGS needs to be specified at the LES domain inlet in order to predict r.m.s at near-field correctly.
- For both isothermal and non-isothermal jets, simulation of precursor is vital, but in contrast to isothermal, DDES implemented in OpenFOAM is not capable of accurately generating inlet condition for non-isothermal jet.
- Far-field data is found to be independent of temperature intensity at the inlet in both experimental and computational approaches.
- LES implemented in the OpenFOAM toolbox is capable of simulating both isothermal and non-isothermal flow over cylinder.

www.manaraa.com

For future work related to the HTGR modeling, additional efforts should be made in order to bridge the gap between fundamental flows such as those studied in this thesis and the complex flow configurations of the actual lower plenum. Specifically, the following studies should be conducted:

- Non-isothermal LES of higher Reynolds number for flow over cylinder;
- Quantification of inlet turbulence intensity on flow over cylinder;
- Effect of span-size of the cylinder and also number of cell divisions on flow over cylinder simulation;
- Comprehensive study of the impact of SGS on both isothermal and non-isothermal LES of jets; and
- Spectral analysis of flow issuing from contraction to find a way to provide accurate but computationally low-cost inlet boundary condition for jet simulation.

In terms of more fundamental contributions to LES, this thesis presents a first step in ultimately quantifying the uncertainty in this important family of flow modeling. Since the canonical flows discussed here now have trusted LES results, the sensitivity and impact of the input parameters, including mesh size and the SGS model, can be quantified. This should ultimately enable standard approaches to be formulated for uncertainty quantification, an enormously worthwhile topic which is relatively unaddressed in the current literature.

www.manaraa.com

BIBLIOGRAPHY

[1] F. Stern, R.V. Wilson, H.W. Coleman, E.G. Paterson, Comprehensive approach to verification and validation of CFD simulations—part 1: methodology and procedures, Journal of fluids engineering, 123 (2001) 793-802.

[2] W.L. Oberkampf, T.G. Trucano, C. Hirsch, Verification, validation, and predictive capability in computational engineering and physics, Applied Mechanics Reviews, 57 (2004) 345-384.

[3] U. DoE, A technology roadmap for generation IV nuclear energy systems, in: Nuclear Energy Research Advisory Committee and the Generation IV International Forum, 2002.

[4] H.M. McIlroy, D.M. McEligot, R.J. Pink, Measurement of flow phenomena in a lower plenum model of a prismatic gas-cooled reactor, Journal of Engineering for Gas Turbines and Power, 132 (2010) 022901.

[5] D. McEligot, K. Condie, T. Foust, G. McCreery, R. Pink, D. Stacey, A. Shenoy, G. Baccaglini, R. Pletcher, J. Wallace, Fundamental Thermal Fluid Physics of High Temperature Flows in Advanced Reactor Systems-Nuclear Energy Research Initiative Program Interoffice Work Order (IWO) MSF99-0254 Final Report for Period 1 August 1999 to 31 December 2002, in, Idaho National Engineering and Environmental Laboratory, Idaho Falls, ID (US), 2002.

[6] S. Mazumdar, A. Jana, M. Kimber, Initial Computational Study of The Thermal Mixing In A VHTR Lower Plenum, in: 15th International Topical Meeting on Nuclear Reactor Thermal hydraulics, Pisa, Italy, 2013.

[7] R.W. Johnson, Modeling strategies for unsteady turbulent flows in the lower plenum of the VHTR, Nuclear Engineering and Design, 238 (2008) 482-491.

[8] R.W. Johnson, D.P. Guillen, T. Gallaway, Investigations of the Application of CFD to Flow Expected in the Lower Plenum of the Prismatic VHTR, Idaho National Laboratory, 2006.

[9] N. Kimura, H. Miyakoshi, H. Kamide, Experimental investigation on transfer characteristics of temperature fluctuation from liquid sodium to wall in parallel triple-jet, International journal of heat and mass transfer, 50 (2007) 2024-2036.

www.manaraa.com

[10] S.B. Pope, Turbulent flows, Cambridge university press, 2000.

[11] P. Sagaut, Large eddy simulation for incompressible flows, Springer, 2002.

[12] N. Panchapakesan, J. Lumley, Turbulence measurements in axisymmetric jets of air and helium. Part 1. Air jet, Journal of Fluid Mechanics, 246 (1993) 197-223.

[13] I. Wygnanski, H. Fiedler, Some measurements in the self preserving jet, Cambridge Univ Press, 1968.

[14] H.J. Hussein, S.P. Capp, W.K. George, Velocity measurements in a high-Reynolds-number, momentum-conserving, axisymmetric, turbulent jet, Journal of Fluid Mechanics, 258 (1994) 31-75.

[15] J. Kim, H. Choi, Large eddy simulation of a circular jet: effect of inflow conditions on the near-field, Journal of Fluid Mechanics, 620 (2009) 383.

[16] C. Bogey, C. Bailly, Turbulence and energy budget in a self-preserving round jet: direct evaluation using large eddy simulation, Journal of Fluid Mechanics, 627 (2009) 129.

[17] A. Clément, Coupling of two absorbing boundary conditions for 2D time-domain simulations of free surface gravity waves, J Comput Phys, 126 (1996) 139-151.

[18] D.A. Lysenko, I.S. Ertesvåg, K.E. Rian, Large-eddy simulation of the flow over a circular cylinder at Reynolds number 3900 using the OpenFOAM toolbox, Flow, turbulence and combustion, 89 (2012) 491-518.

[19] D.A. Lysenko, I.S. Ertesvåg, K.E. Rian, Large-Eddy Simulation of the Flow Over a Circular Cylinder at Reynolds Number 2× 104, Flow, Turbulence and Combustion, 1-26.

[20] J. Smagorinsky, General circulation experiments with the primitive equations: I. The basic experiment*, Monthly weather review, 91 (1963) 99-164.

[21] D. Lilly, A proposed modification of the Germano subgrid-scale closure method, Physics of Fluids A: Fluid Dynamics (1989-1993), 4 (1992) 633-635.

[22] S.-E. Kim, Large eddy simulation using an unstructured mesh based finite-volume solver, in: 34th AIAA fluid dynamics conference and exhibit, Portland, 2004, pp. 1-7.

[23] C. Fureby, G. Tabor, H. Weller, A. Gosman, A comparative study of subgrid scale models in homogeneous isotropic turbulence, Physics of Fluids (1994-present), 9 (1997) 1416-1429.

www.manaraa.com

[24] X. Chai, K. Mahesh, Dynamic-equation model for large-eddy simulation of compressible flows, Journal of Fluid Mechanics, 699 (2012) 385-413.

[25] S. Salkhordeh, S. Mazumdar, D.T. Landfried, A. Jana, M. Kimber, A combined RANS-LES simulation of a turbulent round jet in a large enclosure, Bulletin of the American Physical Society, 58 (2013).

[26] C. Bogey, C. Bailly, Large eddy simulations of round free jets using explicit filtering with/without dynamic Smagorinsky model, Int J Heat Fluid Fl, 27 (2006) 603-610.

[27] Y.O. Han, W.K. George, J. Hjarne, Effect of a contraction on turbulence. Part 1: Experiment, Spectrum, 1 (2005) 11.

[28] P.R. Spalart, Detached-eddy simulation, Annual Review of Fluid Mechanics, 41 (2009) 181-202.

[29] G. Lipari, P.K. Stansby, Review of experimental data on incompressible turbulent round jets, Flow, turbulence and combustion, 87 (2011) 79-114.

[30] A. Wray, A selection of test cases for the validation of large-eddy simulations of turbulent flows, AGARD Advisory Report, 345 (1998).

[31] G. Taub, H. Lee, S. Balachandar, S. Sherif, A direct numerical simulation study of higher order statistics in a turbulent round jet, Physics of Fluids (1994-present), 25 (2013) 115102.

[32] J. Scholten, D. Murray, Unsteady heat transfer and velocity of a cylinder in cross flow—i. Low freestream turbulence, International journal of heat and mass transfer, 41 (1998) 1139-1148.

[33] H. Nakamura, T. Igarashi, Variation of Nusselt number with flow regimes behind a circular cylinder for Reynolds numbers from 70 to 30000, International journal of heat and mass transfer, 47 (2004) 5169-5173.

[34] H. Nakamura, T. Igarashi, Unsteady heat transfer from a circular cylinder for Reynolds numbers from 3000 to 15,000, Int J Heat Fluid Fl, 25 (2004) 741-748.

[35] A. Mani, P. Moin, M. Wang, Computational study of optical distortions by separated shear layers and turbulent wakes, Journal of Fluid Mechanics, 625 (2009) 273-298.

[36] D.A. Lysenko, I.S. Ertesvåg, K.E. Rian, Large-eddy simulation of the flow over a circular cylinder at Reynolds number 2× 104, Flow, turbulence and combustion, 92 (2014) 673-698.

www.manaraa.com

[37] S.-E. Kim, H. Nakamura, Large eddy simulation of turbulent heat transfer around a circular cylinder in crossflow, in: ASME/JSME 2007 5th Joint Fluids Engineering Conference, American Society of Mechanical Engineers, 2007, pp. 233-238.

[38] L. Lourenco, C. Shih, Characteristics of the plane turbulent near wake of a circular cylinder, a particle image velocimetry study, private communication, (1993).

[39] P. Parnaudeau, J. Carlier, D. Heitz, E. Lamballais, Experimental and numerical studies of the flow over a circular cylinder at Reynolds number 3900, Physics of Fluids (1994-present), 20 (2008) 085101.

[40] L. Ong, J. Wallace, The velocity field of the turbulent very near wake of a circular cylinder, Experiments in fluids, 20 (1996) 441-453.

[41] A.G. Kravchenko, P. Moin, Numerical studies of flow over a circular cylinder at ReD= 3900, Physics of Fluids (1994-present), 12 (2000) 403-417.

[42] J. Wissink, W. Rodi, Numerical study of the near wake of a circular cylinder, Int J Heat Fluid Fl, 29 (2008) 1060-1070.

[43] J. Franke, W. Frank, Large eddy simulation of the flow past a circular cylinder at Re D= 3900, Journal of wind engineering and industrial aerodynamics, 90 (2002) 1191-1206.

[44] C. Norberg, Fluctuating lift on a circular cylinder: review and new measurements, J Fluid Struct, 17 (2003) 57-96.

[45] S. Corrsin, A.L. Kistler, Free-stream boundaries of turbulent flows, NACA Washington, DC, 1955.

[46] R. Chevray, N. Tutu, Intermittency and preferential transport of heat in a round jet, Journal of Fluid Mechanics, 88 (1978) 133-160.

[47] L. Chua, R. Antonia, Turbulent Prandtl number in a circular jet, International Journal of Heat and Mass Transfer, 33 (1990) 331-339.

[48] R. Antonia, J. Mi, Temperature dissipation in a turbulent round jet, Journal of Fluid Mechanics, 250 (1993) 531-551.

[49] J. Mi, D.S. Nobes, G. Nathan, Influence of jet exit conditions on the passive scalar field of an axisymmetric free jet, Journal of Fluid Mechanics, 432 (2001) 91-125.

[50] J. Mi, G. Nathan, Statistical properties of turbulent free jets issuing from nine differently-shaped nozzles, Flow, turbulence and combustion, 84 (2010) 583-606.

www.manaraa.com

[51] E. Smith, J. Mi, G. Nathan, B. Dally, The" Round Jet Inflow-Condition Anomaly" for the k-ε Turbulence Model, School of Mechanical Engineering, University of Adelaide (Australia), (2004).

[52] H. Suto, K. Matsubara, M. Kobayashi, Y. Kaneko, Large eddy simulation of flow and scalar transport in a round jet, Heat Transfer—Asian Research, 33 (2004) 175-188.

[53] E. Colombo, F. Inzoli, A. Muzzio, J. Teatini, modelling for free, incompressible and non-isothermal round jets'', in: 5th European Thermal-Science Conference, 2008.

[54] R. So, J. Zhu, M. Ötügen, B. Hwang, Some measurements in a binary gas jet, Experiments in Fluids, 9 (1990) 273-284.

[55] F. Lockwood, H. Moneib, Fluctuating temperature measurements in a heated round free jet, Combustion Science and Technology, 22 (1980) 63-81.

[56] D.R. Dowling, P.E. Dimotakis, Similarity of the concentration field of gas-phase turbulent jets, Journal of Fluid Mechanics, 218 (1990) 109-141.

www.manaraa.com